ADVANCED MATERIALS INTERFACES
www.advmatinterfaces.de

Ferrimagnetic Dynamics Induced by Spin-Orbit Torques

Giacomo Sala and Pietro Gambardella**

Ferrimagnets are the magnetic materials with the fastest current-induced dynamics reported so far. Among them, rare-earth transition-metal (RE-TM) alloys offer a fertile playground for studying the behavior of multi-sublattice systems with tunable composition and magnetic interactions. This review provides a survey of the magnetic dynamics excited by current-induced spin-orbit torques (SOTs) in RE-TM ferrimagnets coupled to heavy-metal layers. It summarizes the magnetic properties of RE-TM alloys and discusses how interfacial SOTs result in efficient magnetization switching and fast domain-wall motion close to the magnetization and angular momentum compensation points. Recent work shows that the switching is a multiphase process affected by significant stochastic fluctuations. However, strong SOTs results in fast and deterministic sub-ns switching with minimal energy dissipation. In addition, the RE and TM magnetizations can respond asynchronously to SOTs during the reversal. This asynchronous dynamics pinpoints the different strength of the SOTs acting on the two sublattices and challenges the usual assumption of rigid inter-sublattice antiferromagnetic coupling. Overall, the ability to tailor the timescale and reversal mode of RE-TM alloys allows for optimizing the speed of ferrimagnetic spintronic devices and provides insight into the current-induced transfer of angular momentum in systems with synergistic ferromagnetic and antiferromagnetic interactions.

1. Introduction

The discovery of current-induced spin torques[1–4] in thin films and at interfaces has revolutionized modern magnetism by providing a scalable, fast, and energy-efficient alternative to magnetic fields to manipulate magnetic moments.[5,6] Spin torques arise from the transfer of angular momentum between two reservoirs mediated by the spin and orbital moments of conduction electrons. In the so-called spin transfer torque (STT), angular momentum is exchanged between two ferromagnets separated by a non-magnetic layer, either conducting or insulating.[4,7] This effect underlies the functionality of magnetic tunnel junctions, the elemental unit of state-of-the-art magnetic memories. However, more effort has been devoted recently to substitute or complement the STT with another form of spin torque, the spin-orbit torque (SOT).[8–13] SOT is a relativistic effect rooted in the spin-orbit interaction that couples the magnetic order to the crystal lattice.[13] This coupling can manifest through different phenomena. Traditionally, SOTs have been attributed to the spin Hall effect occurring in the bulk of nonmagnetic layers[10,14,15] and to the Rashba effect at nonmagnet/ferromagnet interfaces.[8,16–18] The original binary parsing has nowadays been relaxed since several other mechanisms contribute to SOTs, especially at interfaces[13,19–27] and in systems with orbital texture[28–31] or helical surface states.[32–36] Both the STT and SOTs can excite magnetic dynamics such as magnetization precession and switching, but SOTs offer unparalleled possibilities that are precluded to the STT. SOTs are ubiquitous because available in both magnetic and nonmagnetic materials, and can be exerted on both conducting and insulating magnets, whether ferro- or antiferromagnetic. SOTs can also drive magnetic quasi-particles such as domain walls[37–39] and skyrmions[40–43] more efficiently and at higher speeds than the STT, thereby enabling logic functionalities.[44] In the specific case of magnetic tunnel junctions, they also provide important advantages over STT, such as higher endurance, lower read disturbance, and greater design flexibility.[45–53]

The switching of perpendicularly-magnetized films such as the free layer of magnetic tunnel junctions is one of the main applications of SOTs.[9] In general, the magnetization switching is a complex process involving many interrelated magnetic and nonmagnetic parameters (SOTs, saturation magnetization and magnetic anisotropy, damping, Joule heating, device geometry) and nonuniform magnetic configurations (domains and domain walls). Despite this intrinsic complexity, there exist general physical relations between the duration t_p and the minimum amplitude J of the electric current (density) that induces the switching.[55,60,61] In the short-pulse regime ($t_p \lesssim 10$ ns), Joule heating plays a limited role and the switching is governed by the conservation of the interfacial angular momentum transferred to the magnetic system, such that:[45,50,55,56,62]

$$J = J_0 + \frac{q}{t_p} \tag{1}$$

Here, J_0 is the threshold switching current density in the limit $t_p \to \infty$, and q is an effective electric charge density proportional to the required angular momentum. Equation (1) has important implications. The energy dissipated during the electric pulse is $E = RI^2 t_p$, where R is the device resistance, $I = \mathcal{A}J$

G. Sala, P. Gambardella
Magnetism and Interface Physics, Department of Materials
ETH Zurich
Hönggerbergring 64, Zürich 8093, Switzerland
E-mail: giacomo.sala@mat.ethz.ch; pietro.gambardella@mat.ethz.ch

The ORCID identification number(s) for the author(s) of this article can be found under https://doi.org/10.1002/admi.202201622.

DOI: 10.1002/admi.202201622

ADVANCED MATERIALS INTERFACES
www.advmatinterfaces.de

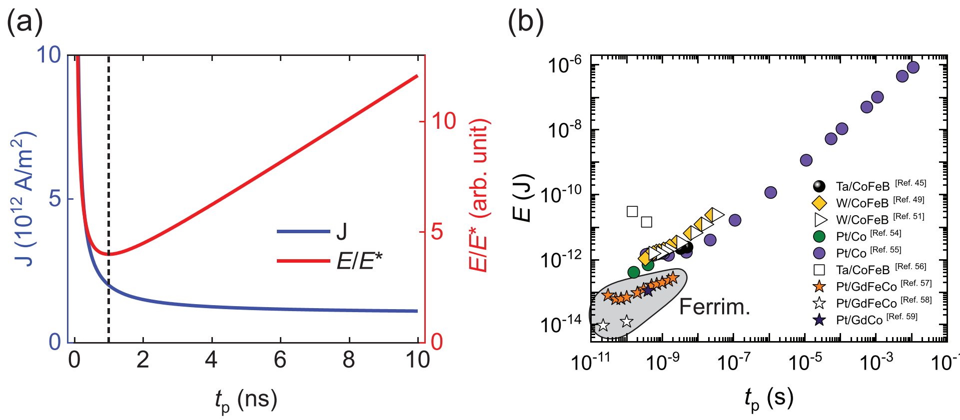

Figure 1. a) Dependence of the threshold switching current density (blue) and energy consumption (red) on the pulse length in the short-pulse regime, as calculated from Equations (1) and (2) with $J_0 = 10^{12}$ A m^{-2}, $q = 10^3$ C m^{-2}. The dashed line indicates the energy minimum at $t_p^* = 1$ ns. b) Energy dissipated by the SOT-induced magnetization switching as a function of the switching time in heavy metal/ferromagnet and heavy metal/RE-TM ferrimagnets. The energy consumption and the switching time were calculated from the data in refs. [45, 49, 51, 54–59] after normalizing the lateral dimensions of the devices to 100 nm.

is the current amplitude, and $\mathcal{A}$ is the surface through which the current flows. Thus, the energy consumed to switch the magnetization scales as

$$E = \left(2 + \frac{t_p}{t_p^*} + \frac{t_p^*}{t_p}\right) E^* \tag{2}$$

where $t_p^* = q/J_0$ and $E^* = R\mathcal{A}^2 q J_0$. Equation (2) shows that the energy consumption decreases initially as $1/t_p$ up to the turning point $t_p = t_p^*$, from which it increases linearly with the pulse length (**Figure 1**). These two opposite trends stem from different physics. The initial decrease with t_p reflects the convenience of using long electric pulses to transfer a fixed amount of angular momentum (q) because the energy dissipation scales quadratically with the pulse amplitude and only linearly with the pulse duration. Instead, the linear increase beyond $t_p = t_p^*$ vanishes in the limit $J_0 \to 0$ and thus implies that J_0 is an intrinsic time-independent loss factor, that is, angular momentum that is not effectively used to switch the magnetization.

Since the energy consumption is minimum at $t_p = t_p^*$, achieving fast and efficient switching requires reducing t_p^*. This optimization cannot involve J_0 since its contribution to t_p^* and E^* is opposite. The only addressable parameter is q, which depends on the SOT efficiency and the saturation magnetization.[61] These considerations suggest that, apart from optimizing the SOT efficiency, a possible way of curbing the energy dissipation is to reduce the saturation magnetization, that is, the required angular momentum. Since typical transition-metal ferromagnets have a large magnetization in the order of 1 MA m^{-1}, antiferromagnets with vanishing net magnetic moment would be ideal candidates. Antiferromagnets, however, have intrinsic drawbacks that limit their use in devices, namely, the difficult control by magnetic fields and the absence of large read-out signals. Ferrimagnets represent instead a good compromise because their unequal magnetic sublattices do not fully compensate each other. They combine a small saturation magnetization and a weak stray field with fast dynamics typical of the antiferromagnetic order. To date, ferrimagnets are indeed the only materials in which record domain wall speeds of several km s^{-1} have been reported.[59,63–65] These advantageous characteristics along with the large tunability of their magnetic properties have raised considerable interest in these materials, which promise faster and more energy-efficient applications than ferromagnets (see Figure 1).[66,67] Particularly interesting are rare-earth transition-metal (RE-TM) ferrimagnetic alloys because they merge the large magnetic moment and single-ion anisotropy of RE atoms with the strong exchange interaction of TM elements. Their distinct atomic elements coincide with the magnetic sublattices. This one-to-one correspondence between the elemental composition and the magnetic order is at the origin of quite a rich and surprising physics, which, despite decades of research, is far from a complete understanding.

In this review, we combine results of recent studies to provide a comprehensive picture of the SOT-induced switching in RE-TM ferrimagnets. We address long-standing open points of the dynamics excited by SOTs in these materials on the ns and sub-ns timescale. In particular, we compare the similarities and differences between the magnetization switching in ferro- and ferrimagnets, the timescales of the reversal, the individual dynamics of the RE and TM magnetizations, and the separate interaction of the two sublattices with SOTs. A deeper comprehension of the ferrimagnetic dynamics is required to pave the way toward ferrimagnet-based spintronic applications and provide insight into the dynamics of multi-sublattice systems.

This review is organized as follows. Section 2 gives an overview of the magnetic properties of RE-TM alloys, including their atomic structure, the magnetic order, the compensation points, and the equations describing their dynamics. Section 3 presents the latest findings on SOTs in RE-TM ferrimagnets, and the SOT-induced motion of domain walls and magnetization switching. Section 4 focuses on the timescales of the magnetization switching and its reproducible and stochastic components, and proposes strategies to combine the fast and reproducible dynamics with low energy consumption. Section 5 discusses the origin and implications of the asynchronous sublattice dynamics revealed by a complementary study of the switching of RE-TM ferrimagnets. Finally, Section 6 summarizes the state

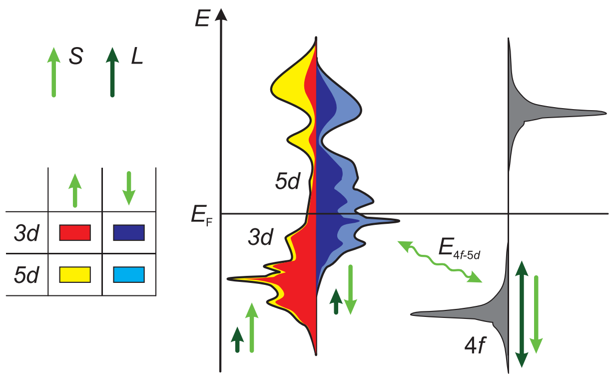

Figure 2. Schematic of the electronic bandstructure of RE-TM alloys at the Fermi level E_F. The colors code for the contributions of RE 5d and TM 3d orbitals to the spin up (majority) and spin down (minority) bands, as indicated in the table on the left.

of the art of the current-induced dynamics in RE-TM ferrimagnets and discusses opportunities and challenges awaiting these materials in the coming years.

2. Magnetic Properties of Rare-Earth Transition-Metal Ferrimagnets

2.1. Band Structure of RE-TM Ferrimagnets

RE-TM ferrimagnets are typically binary or ternary alloys of TM (Co, Fe) and RE elements (mostly Gd, Tb, and Dy). Their ferrimagnetic order originates from bandstructure effects[68–73] and can be understood with the aid of **Figure 2**. Upon alloying, the 3d and 5d bands of the TM and RE elements, respectively, hybridize, but the degree of mixing is different for spin-up (majority) and spin-down (minority) states. The 3d–5d hybridization is stronger for the minority states because their energy separation is smaller. As a consequence, the net spin polarizations of 3d and 5d electrons are antiparallel because most of 3d electrons have their spin up and most of 5d electrons have their spin down. The nature of the RE-TM coupling is then determined by the 4f–5d interaction in conjunction with Hund's third rule in the localized 4f orbitals.[74] These states are the source of the RE magnetism and preserve a large orbital moment. The 4f spins polarize the 5d electrons and establish a ferromagnetic alignment between 4f orbitals and the 5d band ($E_{4f-5d} > 0$). This implies that the spins of the 4f electrons are always antiparallel to the 3d majority electron spins. According to Hund's rule, the "light" RE elements before Gd have antiparallel spin S and orbital L moments. Since $L > S$, the 3d and 4f magnetic moments are parallel: alloys with light RE atoms are ferromagnetic. On the contrary, the "heavy" RE elements after Gd have parallel spin and orbital magnetic moments, thus their net moment is antiparallel to the 3d moment: heavy RE elements induce the ferrimagnetic order. Gd has zero orbital angular momentum ($L = 0$) and the magnetic moment is produced entirely by the spin ($S = 7/2$), thus Gd-based alloys are ferrimagnetic. These rather complex interactions can be condensed in three exchange coupling energies: $E_{\text{RE-RE}} < |E_{\text{TM-RE}}| < E_{\text{TM-TM}}$.[75]

2.2. Compensation Points

Since the atomic composition $\text{RE}_x\text{TM}_{(1-x)}$ can be continuously varied, there is a virtually-unlimited number of ways to tune the magnetic properties of RE-TM compounds. In practice, the benefits of combining RE and TM elements are restricted to a narrow range of compositions, typically with $20 < x < 35$, where the net magnetic moment μ, magnetization M, and angular momentum A approach zero. μ and M are simply given by:

$$\mu(x,T) = |(1-x)\mu_{TM} - x\mu_{RE}| \tag{3}$$

$$M(x,T) = \frac{\mu}{\mathcal{V}} = |M_{TM}(T) - M_{RE}(T)| \tag{4}$$

with $\mathcal{V}$ the magnetic volume. **Figure 3** shows the temperature dependence of the RE and TM magnetizations calculated by

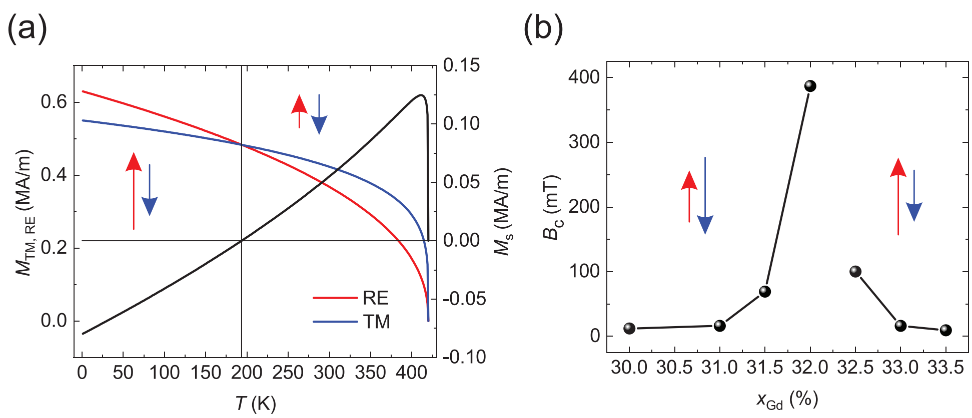

Figure 3. a) Calculated temperature dependence of the RE = Gd (red) and TM = FeCo (blue) magnetizations according to a Bloch-like law: $M(T) = M(0)(1 - T/T_C)^{\beta}$, with $M_{TM}(0) = 0.55$ MA m^{-1}, $M_{RE}(0) = 0.63$ A m^{-1}, $\beta_{TM} = 0.21$, $\beta_{RE} = 0.43$, and Curie temperature $T_C = 420$ K.[76,77] The net magnetization $M_{TM} - M_{RE}$ (black, right vertical axis) vanishes at the characteristic temperature T_M (≈ 190 K in this case). The arrows represent the magnitude and orientation of the sublattice magnetizations. b) Dependence of the coercive field on the Gd concentration measured via the anomalous Hall effect in sputtered $\text{Gd}_x(\text{FeCo})_{1-x}$(15 nm) samples.

a mean-field model.[76,77] Since the RE magnetization is larger at low temperature but decreases more rapidly than the TM magnetization at high temperature because of the intrinsically weak 4f–4f coupling, there exists a composition and a temperature at which the total magnetization vanishes and a fully compensated antiferromagnetic state is established.[78,79] These points are called the magnetization compensation composition x_M and compensation temperature T_M. The divergence of the coercive field in Figure 3 identifies x_M and pinpoints the transition between the RE-dominated and TM-dominated regimes.

Differently from ferromagnets and antiferromagnets, the net magnetization and angular momentum of RE-TM ferrimagnets are distinct quantities because the Landé factors of RE and TM atoms are different ($g_{RE} = 2.0$ and $g_{TM} \approx 2.2$). The Landé factor does not change significantly as the composition or temperature are varied because it depends on the spin and orbital angular momenta of the two atomic species. The atomic momenta do not depend on temperature and are weakly dependent on stoichiometry in bulk-like systems. In particular, the inequality $g_{RE} < g_{TM}$ implies that $T_A > T_M$ and $x_A < x_M$. The existence of the angular momentum compensation is crucial for the ferrimagnetic dynamics. At T_M the net *equilibrium* magnetization vanishes and the magnetic order becomes akin to that of antiferromagnets, yet it is only at T_A that the *dynamics* changes from ferromagnetic to antiferromagnetic. This is because the temporal evolution of magnetic phenomena is ruled by the commutator of the angular momentum, not the magnetization.[80] Thus, RE-TM ferrimagnets offer a unique combination of finite magnetization and antiferromagnetic dynamics, that is, the Néel vector of ferrimagnets can be driven by magnetic fields and SOTs as the magnetization of ferromagnets.

2.3. Magnetic Anisotropy

RE-TM ferrimagnets should have isotropic properties because of their amorphous structure.[81–83] In particular, no net magnetic anisotropy is expected. However, several alloys present a uniaxial anisotropy energy of the form $E = k_1 \sin^2\theta + k_2 \sin^4\theta + \ldots$, with θ the angle between the magnetization and the normal direction, and k_i the energy density. The zero-order contribution $k_1 \approx 1$–100 kJ m^{-3} is often positive, meaning that the orientation out of the plane is favored. The origin of this unexpected anisotropy is controversial and attributed to a number of concomitant factors, which include: the short-range atomic order; the large single-ion anisotropy of RE atoms; the columnar microstructure promoted by particular growth conditions; structural inhomogeneities caused by phase separation and formation of clusters; magnetostriction and anisotropic stress distributions.[76,81–83] Despite its complex and yet not-understood nature, the anisotropy of ferrimagnets is an intrinsic bulk property, in contrast to the anisotropy of ferromagnets, which is often of interfacial origin. Therefore, ferrimagnets do not need a careful engineering of interfaces to attain the out-of-plane orientation. Moreover, since their anisotropy is enhanced in thick films,[84] the stability of the magnetic layer against thermal fluctuations, which scales with the volume, may be larger than in ferromagnets. In principle, the perpendicular anisotropy is possible only close to the magnetization compensation because far from this point the total magnetization is large and the demagnetizing field dominates. However, since the dynamics of ferrimagnets is most interesting close to the compensation point, this theoretical limit does not translate into a practical constraint. These advantages explain the strong interest in employing ferrimagnets for data storage. RE-TM ferrimagnets were indeed among the most promising candidates for magnetoptical recording.[85–88]

2.4. Atomic Structure and Magnetic Disorder

Although RE-TM ferrimagnets can grow as crystals, preparation techniques such as liquid quenching, evaporation, and sputtering result in most cases in amorphous structures. The details of the microstructure depend sensitively on the deposition process, but a common feature of RE-TM alloys is the lack of any long-range order.[76] On the other hand, the similarity between the properties of crystalline and amorphous compounds suggests that the short-range atomic order is not suppressed completely.[89–92] Atomic structures extending over distances of ≈1 nm mediate a seamless transition from the local order to the long-range amorphous configuration. The existence of randomly-oriented nano-crystallites in GdFeCo is confirmed by sharp white spots in nanobeam electron diffraction patterns (**Figure 4**). Averaging several patterns at different sample locations reveals that the crystallites correspond to the hexagonal and cubic phase of Gd and Fe, respectively. Thus, amorphous RE-TM ferrimagnets can host RE-rich and TM-rich segregated clusters with approximately nm size. Such clustering effects are accompanied by significant deviations of the local atomic concentration from the average stoichiometry. The local variation estimated from electron transmission measurements can reach up to 10% relative to the mean, but the maximum deviation may actually be larger than 10% because transmission measurements average over a thickness that is much larger than the fluctuation lengthscale.

Moreover, RE-TM amorphous alloys are metastable, and their structure undergoes continuous atomic rearrangement and interdiffusion.[76] This evolution is corroborated by the comparison of nominally-identical but differently-aged GdFeCo samples. Energy-dispersive X-ray spectroscopy (STEM-EDX) elemental maps reveal that the fresh sample presents a larger degree of anticorrelation between the concentration of Fe and Gd (**Figure 5**). This difference is further supported by electron diffraction measurements, which indicate a median cluster size of about 3.8 nm for both Gd and Fe in the fresh sample, and 3.2 and 3.4 nm for Gd and Fe, respectively, in the aged sample. Thus, we conclude that phase segregation takes place in RE-TM films,[89,90,93–96] but atoms of different species tend to interdiffuse upon aging because the mixing enthalpy of TM and RE atoms is negative.[76,97,98]

This chemical and structural disorder leads to a distribution of the magnitude of magnetic moments, exchange interactions, and local electrostatic fields. Although such a randomization does not prevent the formation of a collective magnetic order, it causes important deviations from the ideal picture of collinear ferro- and ferrimagnets.[76] In particular, the competition between the locally-varying exchange interaction and

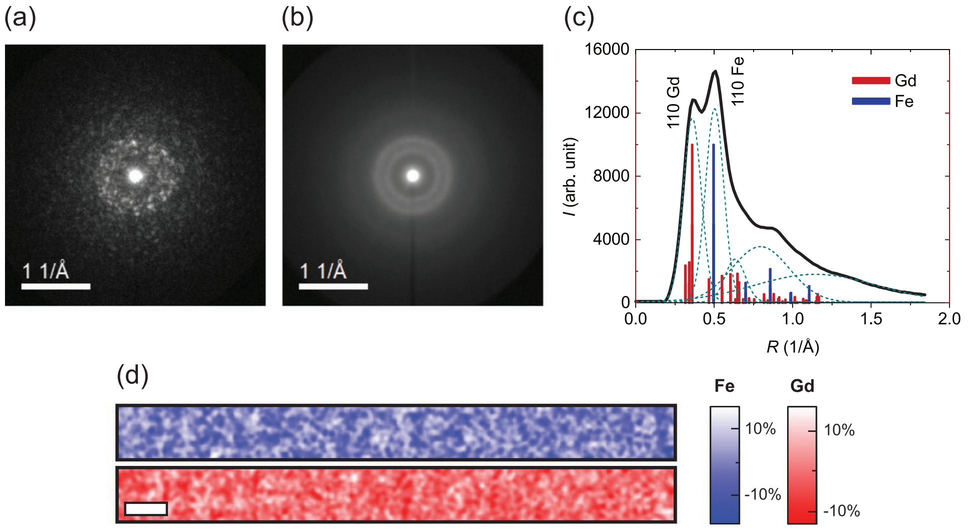

Figure 4. a) Nanobeam electron diffraction pattern of sputtered $Gd_{31}Fe_{62}Co_7$ (15 nm) grown on an amorphous SiN substrate. The white spots indicate the presence of randomly-oriented crystallites. b) Average of 270 such patterns acquired at different equidistant positions in a rectangle of 7×42 nm^2. c) Radially-averaged diffraction intensity profile (black line) obtained from (b). The vertical bars at the bottom are reference patterns of hexagonal Gd (in red) and cubic Fe (in blue). d) Maps of the percentage variation of the Fe and Gd concentrations relative to the mean. The scale bars correspond to 5 nm. Reproduced under the terms of the CC-BY license.[58] Copyright 2022, Springer Nature.

anisotropy randomizes the orientation of magnetic moments. As a consequence, the actual magnetic order of RE-TM ferrimagnets is sperimagnetic.[84,99,100] In sperimagnetism, the magnetic moments of the two sublattices are aligned on average in opposite directions, but their orientation is distributed within a cone, as shown in **Figure 6**. Sperimagnetism can involve only one sublattice or both depending on the elements and their concentration. It is normally caused by large spatial fluctuations of the single-ion anisotropy of the RE atoms and is thus strong in alloys of Tb or Dy. In reality, several measurements evidence the existence of sperimagnetism also in GdFeCo despite the weak anisotropy sourced by Gd atoms.[100–102] This likely indicates that fluctuations of the anisotropy are not uniquely responsible for this complex magnetic order, and that local variations of the exchange interaction may also play an important role.

The amorphous and disordered structure of RE-TM ferrimagnets is not necessarily a disadvantage since it can introduce the inversion asymmetry required for the appearance of SOTs and Dzyaloshinskii–Moriya interaction (DMI), even in single ferrimagnetic layers. The DMI exists in bilayers of heavy metals and ferrimagnets similarly to ferromagnets,[64] however the typically-large thickness of RE-TM ferrimagnets limits the role of interfacial effects. Instead, the DMI can be enhanced by a bulk contribution due to compositional gradients or nonuniformities along the growth direction in combination with the large spin-orbit coupling of RE atoms.[96,103] Such vertical asymmetries can be exploited and engineered to maximize the DMI and even achieve field-free SOT switching.[104]

2.5. Precessional Dynamics

The dynamics of strongly-coupled ferrimagnets can be formally described by an effective Landau–Lifshitz–Gilbert (LLG) equation provided that the Gilbert damping α and the gyromagnetic ratio $\gamma = g\frac{\mu_B}{\hbar}$ are replaced by effective parameters (here μ_B is Bohr's magneton and ħ is Planck's constant).[105–107] If we define the net magnetization in terms of the sublattice magnetizations $\mathbf{M}_1, \mathbf{M}_2$ as $\mathbf{M} = M\mathbf{m} = \mathbf{M}_1 + \mathbf{M}_2$, then the effective LLG equation reads

$$\frac{\mathrm{d}\mathbf{m}}{\mathrm{d}t} = -\gamma_{\text{eff}}\, \mathbf{m} \times \mathbf{B}_{\text{eff}} + \alpha_{\text{eff}}\, \mathbf{m} \times \frac{\mathrm{d}\mathbf{m}}{\mathrm{d}t} \tag{5}$$

$$\gamma_{\text{eff}} = \frac{M_1 - M_2}{\frac{M_1}{\gamma_1} - \frac{M_2}{\gamma_2}} = \frac{M}{A} \tag{6}$$

$$\alpha_{\text{eff}} = \frac{\frac{\alpha_1 M_1}{\gamma_1} + \frac{\alpha_2 M_2}{\gamma_2}}{\frac{M_1}{\gamma_1} - \frac{M_2}{\gamma_2}} = \frac{\alpha_1 A_1 + \alpha_2 A_2}{A} \tag{7}$$

with $\alpha_{1,2}$ and $\gamma_{1,2}$ the damping parameter and the gyromagnetic ratio of the *i*th sublattice, respectively, and $A = \frac{M_1}{\gamma_1} - \frac{M_2}{\gamma_2} = A_1 - A_2$ the net angular momentum ($A_{1,2}$ are assumed always positive). Equations (5)–(7) show that ferrimagnets at the magnetization compensation point behave *statically* as antiferromagnets because $\gamma_{\text{eff}} \to 0$ and the effective field $\mathbf{B}_{\text{eff}}$ becomes uninfluential. In contrast, at the compensation point of the angular momentum, both α_{eff} and γ_{eff} diverge and the *dynamics* becomes very fast, similarly to antiferromagnets. The predicted behavior of the relevant physical parameters of ferrimagnets at the compensation points is summarized in **Table 1**; some of them are discussed in the next section.

The divergences at the compensation points are not physical and stem from treating ferrimagnets on the same ground as

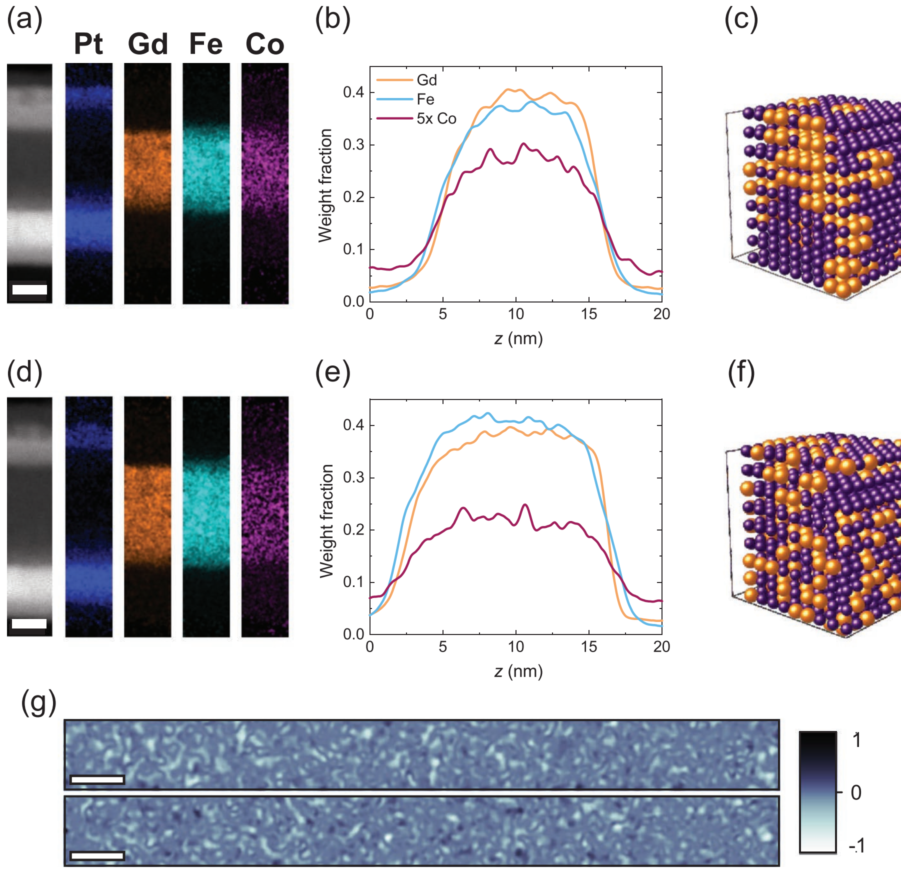

Figure 5. a) STEM-EDX elemental maps of a $Gd_{31}Fe_{62}Co_7$ (15 nm) blanket film 1 month after the growth (fresh sample). b) Profiles of the concentration of Gd, Fe, and Co across the sample thickness. The concentrations of Fe and Gd appear anticorrelated. c) Schematic atomic structure of the sample showing the presence of clusters. The blue (orange) spheres are TM (RE) element atoms. d–f) The same as (a–c) for a nominally-identical sample characterized 30 months after the growth (aged sample). In this case, the concentrations of Fe and Gd show a lower degree of anticorrelation. g) Correlation image of the Fe and Gd concentrations in the fresh (top) and aged (bottom) sample. The larger and more numerous white spots in the correlation image of the fresh sample is indicative of the stronger anticorrelation between the Fe and Gd concentrations. All scale bars correspond to 5 nm. Adapted under the terms of the CC-BY license.[58] Copyright 2022, Springer Nature.

ferromagnets. This is correct close to the magnetization compensation point because the transition occurring there does not have any physical effect other than reversing the quantization axis. Note that the divergence of the coercive field is virtual because the coercive field is not defined in a system without a net magnetization that does not respond to external fields.

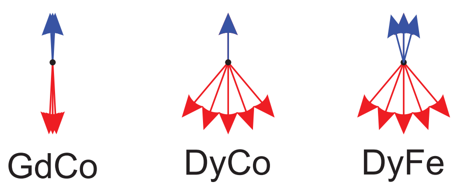

Figure 6. Sperimagnetism of RE-TM alloys. The random electrostatic interactions cause fluctuations of the single-ion anisotropy and result in the distribution of the magnetic moments within a cone (TM moments in blue, RE moments in red). The opening of the cone, called fanning angle, depends on the strength of the exchange interaction and spin-orbit coupling. Ideally, Gd-based alloys do not show significant sperimagnetism because of its small orbital moment, but experiments show that this is not the case. The fanning angle of the TM moments depends also on the specific element.

Moreover, the apparent divergence of the effective SOT fields does not imply an improved torque efficiency, as discussed later. On the other hand, since the dynamics of antiferromagnets is intrinsically different from that of ferromagnets, the standard LLG equation fails in the vicinity of T_A. In this case, an alternative approach consists in describing the dynamics in terms of the Néel vector $\mathbf{n} = \mathbf{M}_1/M_1 - \mathbf{M}_2/M_2$:[67,108,109]

$$A\dot{\mathbf{n}} - \rho\mathbf{n}\times\ddot{\mathbf{n}} - \alpha a\mathbf{n}\times\dot{\mathbf{n}} = \mathbf{f}_{\mathrm{eff}}\times\mathbf{n} \tag{8}$$

where $a = A_1 + A_2$ is the sum of the sublattice angular momenta, ρ is the magnetic inertia, f_{eff} is the energy functional and it is assumed that $\alpha = \alpha_1 = \alpha_2$. Equation (8) correctly describes the dynamics of ferrimagnets and avoids divergences of the resonance frequency, gyromagnetic ratio, and domain wall speed in the proximity of T_A, which corresponds to $A = 0$. The interested reader is referred to ref. [67] and references therein for more details.

It is insightful to consider why the damping is finite and even approximately constant in a range of temperatures around T_A,[80,110] which is not evident in Equation (8). The damping parameter α is a phenomenological quantity that hides all the details of the dissipation processes. Since this dissipation

Table 1. Physical parameters vanishing or diverging at the two compensation points of ferrimagnets when the dynamics is described by the effective LLG Equation (5).

Physical quantity	T_M, x_M	T_A, x_A
Total magnetization	0	finite
Total angular momentum	finite	0
Resonance frequency	finite	∞
Damping	finite	∞
Gyromagnetic ratio	0	∞
Coercive field	∞	finite
Effective SOT fields	∞	finite
Domain wall speed	finite	∞
Anisotropy	finite	finite

involves at the same time both the RE and TM magnetizations, it is not physically correct to define two separate damping parameters $\alpha_{1,2}$, one for each sublattice. If the global loss of angular momentum is taken into account through the Rayleigh function,[80,111,112] then it is possible to show that the total damping of a ferrimagnet becomes

$$\alpha \approx \alpha_{\mathrm{eff}} \frac{A}{A_1 + A_2} \tag{9}$$

and thus remains finite at the compensation point.

Similar to the damping, the resonance frequency of ferrimagnets is also finite at T_A. However, pump-probe laser experiments do show that the characteristic frequency of the ferromagnetic exchange mode (≈10 GHz) is maximum at the angular momentum compensation point because $f_{\mathrm{FMR}} = \gamma_{\mathrm{eff}} B_{\mathrm{eff}}$.[113] In contrast, the frequency of the antiferromagnetic exchange mode, which is normally in the THz range, attains its minimum at this point, where it decreases to ≈70 GHz.[113]

3. Domain Wall Motion and Switching Induced by Spin-Orbit Torques

3.1. SOT in Ferrimagnet/Heavy Metal Bilayers

Similar to ferromagnets, the most common way to generate SOTs in a ferrimagnet is to run an electric current through an adjacent heavy-metal layer such as Pt.[13,106,114–118] Owing to the spin accumulation generated at the ferrimagnet/heavy metal interface by the spin Hall effect in the heavy metal and spin-orbit scattering, a spin current flows into the ferrimagnet. The spin accumulation and the absorption of the spin current result in the field-like (FL) and damping-like (DL) SOTs, respectively, which are given by:[11,13]

$$\mathbf{T}_{\mathrm{FL}} = B_{\mathrm{FL}} \mathbf{M} \times \mathbf{y} \tag{10}$$

$$\mathbf{T}_{\mathrm{DL}} = B_{\mathrm{DL}} \mathbf{M} \times (\mathbf{y} \times \mathbf{m}) \tag{11}$$

The two torques excite the magnetization of ferrimagnets and enable its switching as well as the motion of domains walls. These effects are qualitatively akin to those occurring in ferromagnets. However, the physics of SOTs in RE-TM ferrimagnets is richer and more complex than in ferromagnets because of their multi-sublattice nature. As discussed in the following, this complexity stimulated studies of the dependence of SOTs on the compensation of the magnetization and angular momenta, and on the strength of the torques acting on the individual sublattices.

The finding of enhanced SOTs at the magnetization compensation point aroused initial enthusiasm because it seemed to promise the efficient control of ferrimagnets. Several publications reported that the SOT effective fields diverge at the magnetization compensation temperature (composition) with an inverse dependence on the net magnetization,[106,114–118] in qualitative analogy to the coercive field. Although some measurements indicated a possible contribution of the exchange torque between the two sublattices to the effective SOTs,[119] it is now clear that the apparent divergence of SOTs at T_M does not translate into an improved torque efficiency. This can be explained by adding the field-like and damping-like components of SOTs to the effective LLG model:

$$\frac{d\mathbf{M}}{dt} = -\gamma_{\mathrm{eff}} \mathbf{M} \times (\mathbf{B}_{\mathrm{eff}} + B_{\mathrm{FL,eff}} \mathbf{y}) - \gamma_{\mathrm{eff}} B_{\mathrm{DL,eff}} \mathbf{M} \times (\mathbf{y} \times \mathbf{m}) + \alpha_{\mathrm{eff}} \mathbf{M} \times \frac{d\mathbf{m}}{dt} \tag{12}$$

$$B_{\mathrm{FL,eff}} = \frac{B_{\mathrm{FL,1}} M_1 - B_{\mathrm{FL,2}} M_2}{M_1 - M_2} \tag{13}$$

$$B_{\mathrm{DL,eff}} = \frac{B_{\mathrm{DL,1}} M_1 + B_{\mathrm{DL,2}} M_2}{M_1 - M_2} \tag{14}$$

Here we assume that the current flows along x and the polarization direction of the spin accumulation is along y, and $B_{\mathrm{DL/FL,i}}$ are the SOT fields on sublattice i. Equations (12)–(14) show that the product $MB_{\mathrm{DL/FL,eff}}$ remains finite in the limit $T \to T_M$. Therefore, the torque efficiency $\xi \propto MB_{\mathrm{DL/FL,\ eff}}$ is constant, as required by the conservation of angular momentum.[118,120] This result is confirmed by the independence of the switching current from the magnetization compensation.[106]

We also note the existence of an important difference between the two torque components. Since the general expression of the damping-like (field-like) torque is even (odd) in the magnetization $\mathbf{m}$, the effective damping-like (field-like) field is a weighted sum (difference) of the fields acting on the individual sublattices. As a consequence, the damping-like (field-like) field can (cannot) drive the dynamics of ferrimagnets close to T_M. Therefore, the field-like field behaves similarly to a global magnetic field, which is ineffective in compensated ferrimagnets.

3.2. Domain Wall Motion

One of the most powerful capabilities of SOTs is the possibility of driving domain walls in perpendicularly-magnetized layers at much larger speed than the STT.[121] Efficient motion, however, requires the domain wall to be of Néel type because the internal magnetization of Bloch walls is parallel to the spin polarization.[122,123] Néel walls can be stabilized by applying magnetic fields or by the DMI.[37–39,44,124] In the former case, up-down and down-up domain walls move in opposite directions, and SOTs

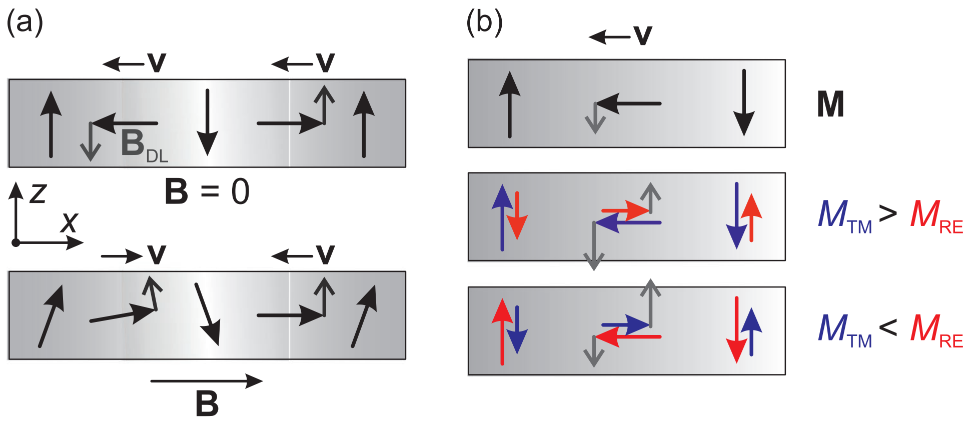

Figure 7. a) Upper panel: SOT-driven motion of ferromagnetic up-down and down-up Néel walls stabilized by the DMI. Lower panel: SOT-driven motion in the presence of a magnetic field stabilizing the internal magnetization of the domain wall. The domain wall speed **v** is the same (opposite) for up-down and down-up Néel walls in the upper (lower) panel. Only the action of the damping-like field is considered because the field-like field cannot drive alone domain walls. b) SOT-driven motion of a ferrimagnetic domain wall in the presence of DMI. Irrespective of whether $M_{TM} > M_{RE}$ (middle panel) or $M_{TM} < M_{RE}$ (bottom panel), the direction of motion remains the same when defined relative to the net magnetization (upper panel). SOT on the TM sublattice is assumed to be stronger than on the RE sublattice.

realize a global switching of the magnetization (**Figure 7**). In the latter case, instead, up-down and down-up domain walls move in the same direction, thus enabling the basic functionality of racetrack devices.[125] This mechanism is common to ferro- and ferrimagnets at any temperature. However, as the angular momentum compensation point is approached, the SOT-driven domain wall motion becomes more efficient in ferrimagnets because domain walls move as rigid objects without internal precession, as discussed below. We notice that the direction of motion in ferrimagnets depends on the sign of the damping-like SOT and DMI/magnetic field as in ferromagnets, but not on the dominant sublattice (Figure 7). Therefore, domain walls of a given type (up-down or down-up) move in the same direction irrespective of whether $M_{TM} > M_{RE}$ or $M_{TM} < M_{RE}$ when the direction of motion and the type are defined relative to the net magnetization.[107,126] The same conclusion holds in the case in which the damping-like SOT acts differently on the two sublattices.

The field- and current-induced motion of domain walls is limited in general by the coupling between the translation of the domain wall and the precession of its internal magnetization, which eventually leads to the Walker breakdown in the strong-drive regime.[127,128] Below this point, the steady-state drift v and precessional ω velocities induced by a magnetic field are given by[63]

$$v = \frac{\alpha a \Delta M B}{A^2 + (\alpha a)^2} \tag{15}$$

$$\omega = \frac{AMB}{A^2 + (\alpha a)^2} \tag{16}$$

where Δ is the width of the domain wall and B the effective driving field. Equations (15) and (16) indicate that the similarity between ferro- and ferrimagnetic domain walls breaks down at the angular momentum compensation point. In a ferromagnet, the angular momentum A is finite at any temperature, and the translational motion of a domain wall is always accompanied by a rotation of its internal magnetization, even in the presence of DMI.[127–129] In contrast, A decreases in a ferrimagnet as T_A (x_A) is approached, which results in the suppression of the precession ($\omega \to 0$) and the maximization of the translational velocity.[107,130] In other words, at the compensation point all the supplied energy is used to drive the domain wall without distorting its internal configuration. Experiments confirm this understanding for both the field- and current-driven dynamics, even if the equations of the current-driven motion are different from Equations (15) and (16),[64,108] which only describe the action of an external magnetic field.[63] As shown in **Figure 8**, the domain wall speed is maximized in correspondence of T_A and can exceed 1 km s^{-1}.[59,63–65] Note that at low current density the velocity may not peak exactly at T_A because the motion is in the linear regime and the sum of the sublattice angular momenta a dominates the net angular momentum A.[64,65] In contrast, at large current density the domain wall speed saturates except at T_A. The possibility of driving fast antiferromagnetic-like dynamics with magnetic fields and SOTs is a unique fingerprint of ferrimagnets with no equivalent in other magnetic materials and is in principle not limited to domain walls. We expect similar considerations to be valid for other quasi-particles such as skyrmions and for spin waves.[131,132] However, although experiments have verified that the so-called skyrmion Hall angle vanishes at T_A,[133,134] experimental evidence of fast skyrmion motion is still lacking.[43] Moreover, fast dynamics at T_A can also be stimulated by effective driving forces other than magnetic fields and SOTs, for example by STT[135,136] or by modulating the magnetic anisotropy of a nanowire by voltage gating.[137] Thus, the fast dynamics at the angular momentum compensation point is a general characteristic of ferrimagnets with promising applications in spintronics. In particular, ferrimagnets may be better candidates than ferromagnets and antiferromagnets to realize fast and energy efficient data storage and logic operations[138] because of the combination of rapid dynamics, low sensitivity to external fields, perpendicular magnetic anisotropy, and large magnetoresistance.

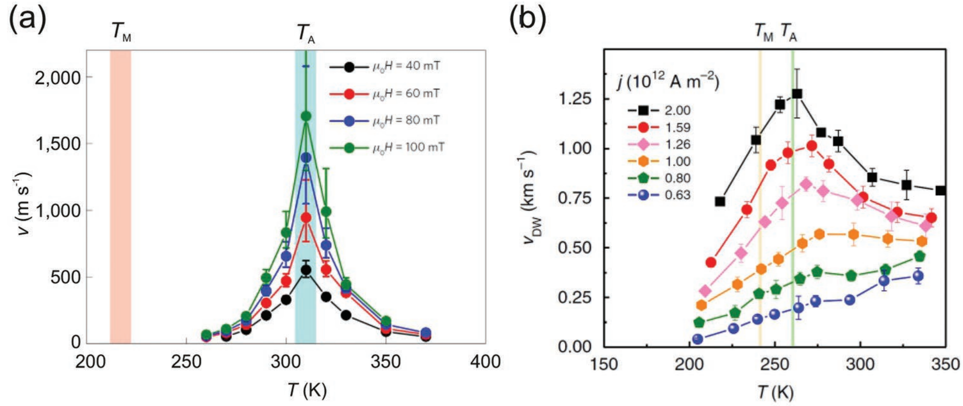

Figure 8. a) Domain wall speed as a function of temperature at different magnetic fields in GdFeCo. Reproduced with permission.[63] Copyright 2017, Springer Nature. b) Domain wall speed as a function of temperature at different current densities in GdCo. Reproduced with permission.[64] Copyright 2018, Springer Nature. The compensation temperature of the magnetization T_M and angular momentum T_A is indicated in both graphs.

Equation (15) does not set any upper limit to the domain wall speed, which increases with the strength of the effective driving field B. Recent theoretical and experimental results contradict this scenario and suggest that the speed of domain walls is limited by a contraction of their width akin to the Lorentz contraction in the theory of special relativity.[108,139] Light speed is in this case replaced by the magnon group velocity. Experimental evidence is so far limited to a ferrimagnetic garnet (BiYIG) with an upper bound velocity of 4.3 km s^{-1}, but RE-TM ferrimagnets are also expected to manifest relativistic dynamics. The maximum achievable speed in these materials remains an open question since it scales with a^{-1}, which is not a directly measurable and easy to estimate parameter.

3.3. Magnetization Switching

Similarly to ferromagnets, SOTs can switch the magnetization (and Néel vector) of ferrimagnets, as shown in **Figure 9**. Here, 1-ms-long current pulses invert the orientation of the magnetization along the normal direction, thereby causing abrupt variations of the anomalous Hall resistance. In a typical heavy metal/ferrimagnet sample such as Pt/GdFeCo, this requires the application of an external field collinear to the current direction to break the mirror symmetry and define the switching polarity.[13]

As discussed in more detail later, the switching comprises an initial quiescent phase associated with the nucleation of a domain and the ensuing domain expansion by domain wall motion. These two processes are SOT-driven, but also thermally-assisted. Since temperature varies on the same timescale as the magnetization switching, the net magnetization and angular momentum are dynamical quantities. Therefore, one or both compensation temperatures may be reached and overcome during the switching,[140,141] and assessing the importance of the two compensation points is challenging.

The compensation of the angular momentum should accelerate the overall switching via the increase of the domain wall speed, but its influence on the domain nucleation remains an open question. The magnetization compensation has also a controversial role. On the one hand, the phenomenological considerations made in Section 1 suggest that compensated ferrimagnets require less energy to switch at the ns timescale because of the reduced effective charge q.[61] However,

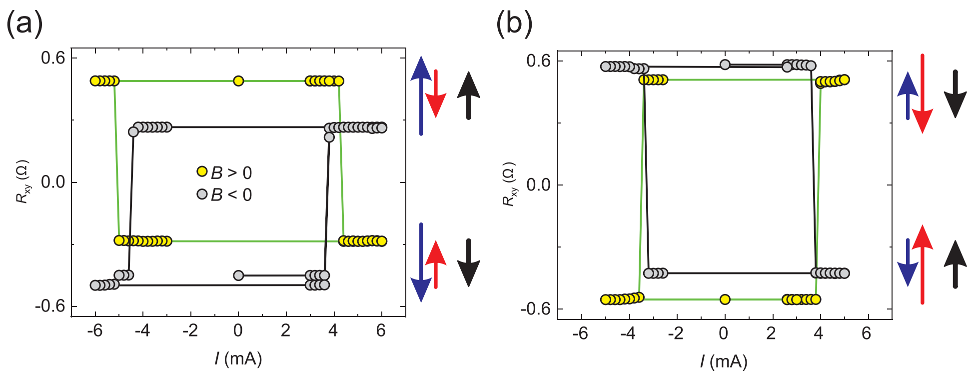

Figure 9. Current-induced switching of the magnetization in Pt/GdFeCo. a) Switching tracked by the anomalous Hall resistance in the presence of an assisting magnetic field along the x direction in a FeCo-dominated Pt(5 nm)/$Gd_{27}(Fe_9Co_1)_{73}$(15 nm) sample. b) The same as (a) in a Gd-dominated Pt(5 nm)/$Gd_{37}(Fe_9Co_1)_{63}$(15 nm) sample. The blue, red, and black arrows indicate the orientation along z of the FeCo, Gd, and net magnetization, respectively. Note that the anomalous Hall resistance changes sign across the magnetization compensation point and is therefore opposite in (a) and (b). Unpublished data by the authors.

whether q is minimum at the magnetization or angular momentum compensation point is still unclear. On the other hand, the enhancement of SOTs at T_M is not accompanied by the increase of the SOT efficiency, and the switching current J is not minimized at the magnetization compensation, at least when using ms-long electric pulses.[106] Moreover, Equation (12) shows that the SOT-induced dynamics is not affected by the compensation of the magnetization since it neither slows down nor speeds up. We also notice that the switching polarity does not change at T_M when defined with respect to the *net* magnetization. This is demonstrated in Figure 9. In the TM-dominated $Pt/Gd_{27}(Fe_9Co_1)_{73}$ sample, the positive current and positive field switch the net magnetization and the FeCo sublattice from up ($+z$) to down ($-z$), similarly to Pt/ferromagnet bilayers. In the RE-dominated $Pt/Gd_{37}(Fe_9Co_1)_{63}$ sample, instead, the FeCo (Gd) sublattice is switched to the up (down) state, which results again in the up-to-down reversal of the net magnetization. Therefore, the switching polarity remains the same despite the opposite sense of rotation of the hysteresis loops of the two samples, which probe the orientation of the FeCo sublattice. We can thus conclude that the magnetization compensation point has little influence on the efficiency of SOTs and speed of the dynamics, but may have an impact on the energy efficiency. Working at this compensation point is certainly beneficial to reduce the stray field and susceptibility to external fields.

Finally, we note that recent experiments have reported longer spin coherence length in ferrimagnets compared to ferromagnets.[142,143] The spin coherence length, namely, the distance over which injected spins dephase, is limited to a few $\dot{A}$ in ferromagnets, and results in the ~$1/t_{FM}$ dependence of SOTs.[13] In contrast, the antiparallel alignment of magnetic moments in compensated ferrimagnets limits the dephasing because the two magnetic sublattices determine opposite precession directions of the injected spins.[144] It was argued that a longer spin coherence in ferrimagnets weakens the $1/t_{FM}$ scaling and allows for switching thick ferrimagnets with a moderate current density, as indeed experimentally reported.[57,117]

3.4. Open Questions

The vast majority of studies on ferrimagnets employed techniques that do not provide information on the dynamics. The harmonic detection of SOTs, the measurement of the domain wall displacement, and the magnetization switching with ms-long pulses only sense the steady-state response to SOTs. This limitation has left open questions on the actual dynamics and its characteristic spatial and temporal scales. Moreover, previous studies could not conclude on the degree of interaction of the spin current attendant to SOTs with the individual RE and TM sublattices, that is, the relative strength of $B_{DL/FL,1}$ and $B_{DL/FL,2}$. Finally, all existing models of current-induced dynamics in RE-TM ferrimagnets have considered a rigid coupling between the two sublattices, but this assumption has never been tested because very few techniques provide the elemental sensitivity required to disentangle the dynamics of the RE and TM magnetizations. In the next sections, we discuss two recent studies that addressed these questions.

4. Timescales of the Switching Dynamics

4.1. Multiphase Switching Dynamics

The dynamics induced by SOTs can be studied by detecting real-time changes of the anomalous Hall resistance caused by the motion of the magnetization. The procedure consists of recording the anomalous Hall signal during the application of the ns-long electric pulses that trigger the movement of the magnetization, as described in detail in ref. [57]. Time-resolved Hall measurements prove particularly useful for investigating the SOT magnetization switching.

Figure 10 shows exemplary measurements of the switching of a 1-µm-wide circular dot of FeCo-dominated $Gd_{30}Fe_{63}Co_7$ with perpendicular magnetization, patterned on top of a 5-nm-thick Pt Hall bar. The time-resolved Hall signal averaged over multiple switching events indicates a multiphase dynamics that comprises an initial quiescent state, the reversal phase, and the final equilibrium state, with the magnetization remaining constant both before and after the reversal. The observation of a long quiescent phase is surprising because the orthogonality between SOTs and the magnetization should avoid the incubation phase typical of the STT.[55,145–147] Instead, these measurements reveal that the duration of this phase is a significant fraction of the total switching time.

The comparison with ferromagnetic tunnel junctions[49] suggests that the quiescent phase is a characteristic of the thermally-activated regime. In this regime, SOTs are not strong enough to push the magnetization over the anisotropy energy barrier. However, since the temperature increases during the pulse and the magnetic anisotropy is temperature-dependent, the barrier lowers with time and eventually lets the switching start. By increasing the pulse amplitude or the in-plane field, the duration of the quiescent phase is significantly reduced as the switching dynamics approaches the intrinsic regime and thermal effects become less important. Simulations and experiments indicate that this initial phase is associated with the reversal of a seed domain at the device edge.[54,58,148,149] Therefore, we refer to the duration t_0 of this process as the nucleation time. Further, we designate the transition time Δt as the duration of the transition between the up and down signal levels,[150] such that the total switching time is given by $t_0 + \Delta t$. Δt is associated with the expansion of the nucleated domain across the device and is thus a measure of the domain wall speed.

This physical interpretation of t_0 and Δt in terms of domain nucleation and expansion is supported by the measurements presented in the next section. It reveals that the SOT-induced switching of ferrimagnets involves the same phases as that of ferromagnets.[49,54] The ns-long nucleation time is particularly noteworthy because it contrasts with the general expectation of fast dynamics in ferrimagnets. However, the nucleation is determined by Joule heating, which is independent of the ferro- or ferrimagnetic nature of the device, and is thus unavoidable. On the other hand, the domain wall velocity inferred from Δt *is* in the order of a few km s^{-1}, much larger than in ferromagnets. We then conclude that t_0 is the veritable bottleneck of the dynamics, and that fully exploiting the rapidity of ferrimagnets requires finding approaches to suppress the initial quiescent phase.

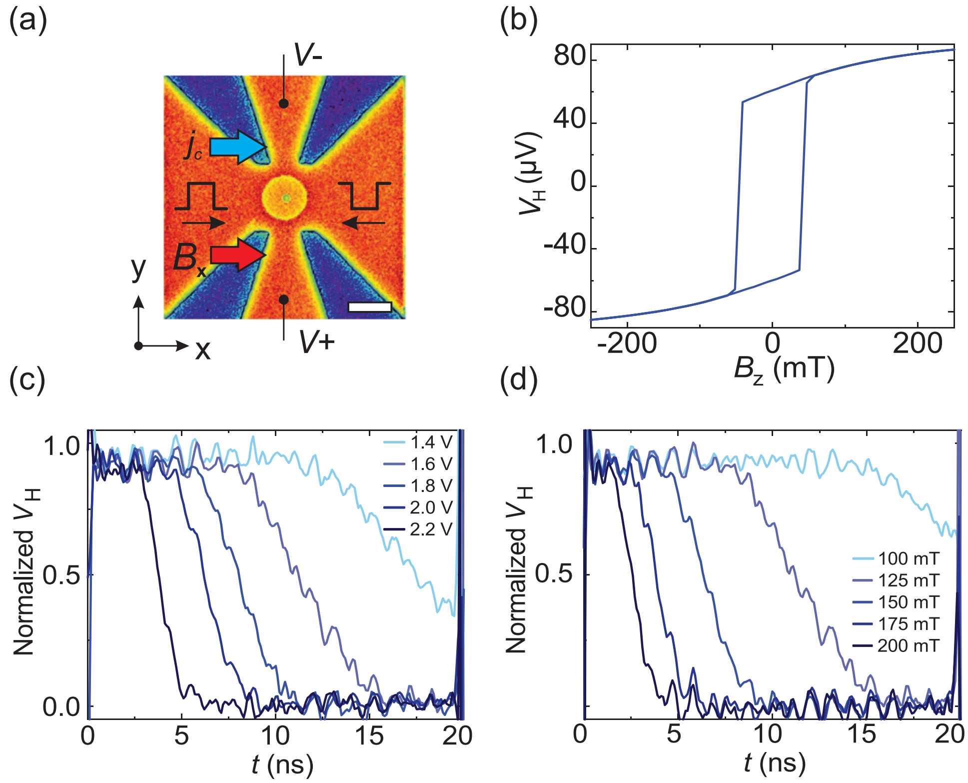

Figure 10. a) False-color scanning electron micrograph of a 1-µm-wide ferrimagnetic $Gd_{30}Fe_{63}Co_7$ (15 nm) dot at the center of a Pt (5 nm) Hall cross. The in-plane magnetic field B_x is collinear to the current. The scale bar corresponds to 1 µm. b) Out-of-plane hysteresis loop detected by measuring the anomalous Hall voltage. c) Normalized averaged switching traces of the GdFeCo dot for 20-ns-long voltage pulses of increasing amplitude. The pulse starts at time 0 and ends at 20 ns, and the magnetic field is 125 mT. d) The same as (c) as a function of the in-plane magnetic field and at constant 1.6 V pulse amplitude. Adapted under the terms of the CC-BY license.[57] Copyright 2021, Springer Nature.

4.2. Stochastic Switching

Since temperature plays such an important role, thermal fluctuations can introduce stochastic effects. The single-shot measurements in **Figure 11** confirm this intuition. The single-shot traces are qualitatively similar to the average traces. However, the duration of the quiescent and transition phases varies significantly from event to event. By fitting each trace to a piecewise linear function, it is possible to extract the statistical distribution of t_0 and Δt (**Figure 12**). The comparison between the single-shot statistics and the averaged traces reveals that the duration of the quiescent phase is systematically underestimated in the average measurements relative to the mean t_0, whereas the duration of the transition phase is systematically overestimated relative to the mean Δt. The quantitative disagreement is determined by the superposition of widely-distributed nucleation events. As shown by the average curves at the bottom of Figure 11, the large spread of the nucleation events anticipates the starting point of the average dynamics and, at the same time, broadens the apparent switching duration.

Significant thermal fluctuations may impair the operation of devices based on SOTs. Strategies are thus needed to mitigate stochastic effects as well as to reduce t_0, as discussed before. Interestingly, increasing the pulse amplitude and/or the magnetic field leads to a reduction of the stochasticity, especially for t_0, whose distributions become narrower as either driving parameter is increased (Figure 12). This hints at a possible approach to make the dynamics faster and more deterministic.

4.3. Favorable Energy Scaling

After-pulse measurements of the threshold switching voltage V_c as a function of the pulse duration t_P evidence the existence of two switching regimes (**Figure 13**). Above ≈5 ns, V_c changes weakly with t_P, which is a signature of the thermally-assisted reversal[55,61] and reveals the importance of thermal effects for the typical pulse lengths and amplitudes used in this study (t_P = 20 ns). On the other hand, the critical voltage increases abruptly for t_P < 3 ns, as expected in the intrinsic regime where the switching speed depends on the rate of angular momentum transfer from the current to the magnetic layer (cf. Figure 1). Indeed, in this regime, V_c scales proportionally to $1/t_P$. Switching with t_P = 300 ps (equivalent average domain wall speed > 3.3 km s^{-1}, under the assumption $t_0 \approx 0$) demonstrates that the quiescent phase can be suppressed by strongly driving the magnetization. Moreover, the statistical trends in Figure 12 prove that short pulses and proportionally-higher voltages improve the reproducibility of the dynamics. Importantly, more intense pulses do not imply a larger energy consumption because the threshold energy density decreases by more than four times upon reducing t_P from 20 ns to < 1 ns.

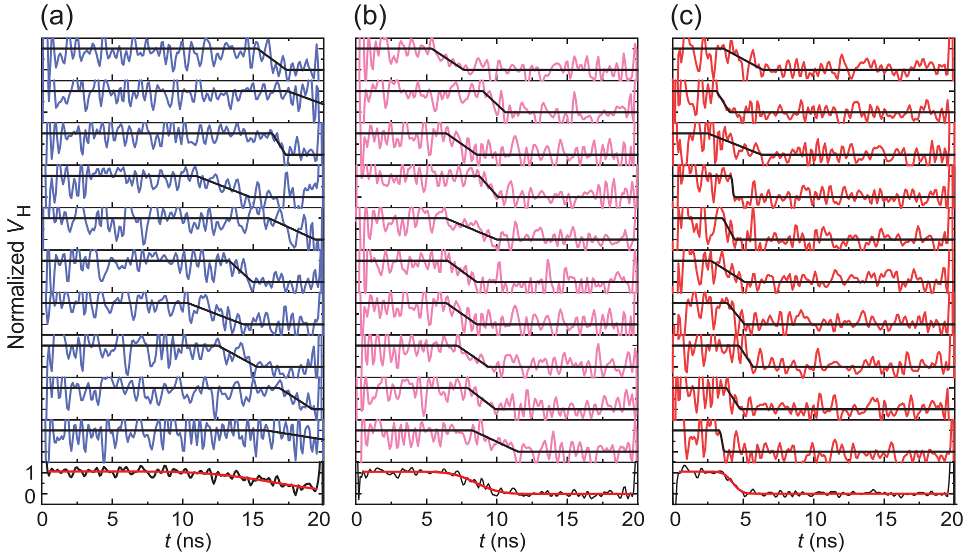

Figure 11. Normalized single-shot traces of the switching of the same GdFeCo device as in Figure 10. The pulse amplitude is 1.4, 1.8, and 2.2 V in (a–c), respectively, and the magnetic field is 125 mT. The black lines are fits to the traces with a piecewise linear function. The bottom-most curve in each graph is the average of the ten traces above, fitted with the cumulative Gaussian function (red). Reproduced under the terms of the CC-BY license.[57] Copyright 2021, Springer Nature.

The conclusions of this study are therefore manifold. The switching dynamics of ferro- and ferrimagnets are qualitatively similar and share the same phases.[49] The overall switching speed is strongly limited by the initial nucleation process, and both the nucleation and the domain expansion are affected by thermal fluctuations. However, the concomitant increase of the pulse amplitude and reduction of the pulse length benefits the speed and reproducibility of the switching without a higher energy demand, at least down to 400 ps. This favorable trend highlights the advantage of using materials with combined fast dynamics and low saturation magnetization.

5. Element- and Time-Resolved Switching of the Rare-Earth and Transition-Metal Magnetizations

5.1. Asynchronous Switching in Time and Space

The measurements discussed in the previous section reveal the characteristic timescales and stochastic nature of the current-induced dynamics of RE-TM ferrimagnets, but do not provide information on the spatial dynamics and the separate behavior of the RE and TM sublattices. These open points can be addressed using the spatial, temporal, magnetic, and element-resolving power of X-rays.[151] In the following, we discuss the results of current pump, X-ray probe measurements performed in a scanning transmission X-ray microscope (STXM).[58]

These measurements disclosed surprising dynamics, as shown in **Figure 14**. Here, the XMCD (X-ray magnetic circular dichroism) intensity integrated over the dot area represents the time dependence of the Fe and Gd magnetizations in a $Gd_{31}Fe_{62}Co_7$ dot excited by 200-ps long electric pulses. The rapid variation of the XMCD signal in correspondence of the electric pulses pinpoints the SOT-induced switching of the magnetization and confirms the fast current-induced dynamics of ferrimagnets. However, the reversal path followed by Fe and Gd is unexpected and very different from the switching trajectory observed in ferromagnets in similar experimental conditions.[54] First, the rapid variation of the XMCD signal is followed by a slow evolution toward equilibrium. Second, although both sublattices share this complex dynamics, they switch asynchronously with respect to each other. In particular, $\mathbf{M}_{Fe}$ reverses its direction during the electric pulse, while $\mathbf{M}_{Gd}$ maintains initially its original orientation. As a consequence, the two magnetizations attain an average transient ferromagnetic state on the ns timescale.

Measurements in more than 20 devices with different elements, concentrations, layer thickness, and lateral size showed that the degree of coupling between the RE and TM sublattices and hence the dynamics can vary significantly, but can be categorized into three types,[58] as reported in **Figure 15**. In general, the reversal of $\mathbf{M}_{Fe}$ always involves the nucleation of a domain at the edge of the dot and the motion of a domain wall across the device with a speed of the order of 1 km s^{-1} depending on the applied current density. This behavior stems from the interplay of SOTs, DMI, and magnetic field, in analogy to ferromagnetic systems.[54,148] In contrast, the temporal and spatial dynamics of the Gd sublattice changes radically from type I to type III.

In the type I, the switching of $\mathbf{M}_{Gd}$ is very different from and substantially slower than that of $\mathbf{M}_{Fe}$. No clear domain wall appears during the pulse, and the progressive change of magnetic contrast is indicative of a turbulent and nonreproducible process. Because of their different speed, $\mathbf{M}_{Fe}$ and $\mathbf{M}_{Gd}$ attain the same orientation during the pulse. The antiferromagnetic order is then re-established only 1 ns after the pulse.

In the type II dynamics, domain walls move in both sublattices but maintain a small relative delay of about 200 ps. Their profiles across the device are also different. Thus, the inter-sublattice coupling appears to be stronger than in the type I switching, but not enough to enforce synchronicity. Instead,

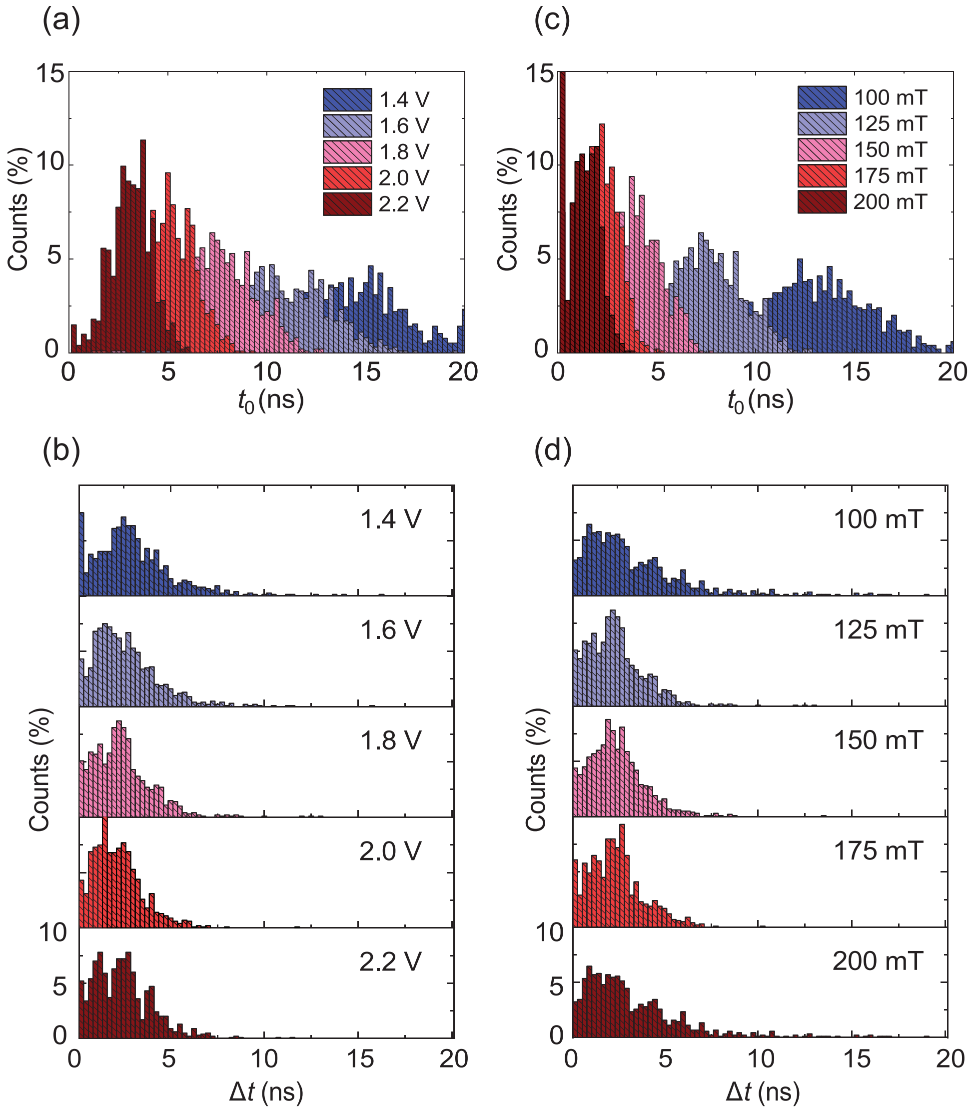

Figure 12. a,b) Statistical distributions of the nucleation time t_0 and transition time Δt for different amplitudes of 20-ns long voltage pulses at a constant in-plane magnetic field of 125 mT. c,d) Same as (a,b), for different in-plane fields at a constant pulse amplitude of 1.8 V. The distributions were obtained by analyzing the single-shot measurements in Figure 11. Reproduced under the terms of the CC-BY license.[57] Copyright 2021, Springer Nature.

the type III is characterized by a strong coupling because $\mathbf{M}_{\mathrm{Fe}}$ and $\mathbf{M}_{\mathrm{Gd}}$ preserve the antiparallel orientation throughout the whole process, both during the edge nucleation of a domain and during its expansion through the device. The type III corresponds to the scenario normally assumed in the modeling of current-induced switching and domain wall motion in ferrimagnets, namely, the rigid antiferromagnetic coupling between the two sublattices.

The stoichiometry of GdFeCo and the pulse amplitude/duration in Figure 15 differ from one device to another. This variation might suggest a relation between the three types of dynamics and the composition and/or electrical excitation. However, the extensive characterization of these dynamics confirmed that each switching type is an intrinsic sample property, independently of the amplitude and duration of the electric pulses as well as of the applied magnetic field, and is not determined by Joule heating.[58] In addition, the type of dynamics is not simply associated with the sample stoichiometry because devices with equal composition showed distinct reversal regimes. More importantly, the additional observation of dynamics of type I and III in TbCo multilayers and alloys (see ref. 58) is a strong indication of the universal character of the asynchronous response of RE-TM ferrimagnets to electric pulses. This generality hints at more fundamental reasons to the asynchronicity than the sample composition and the specific experimental conditions.

5.2. Master-Agent Spin-Orbit-Torque Dynamics

Micromagnetic simulations based on two coupled LLG equations were carried out to identify the origin of the asynchronous dynamics and the reason for the existence of multiple switching paths. As shown in **Figure 16**, the experimental

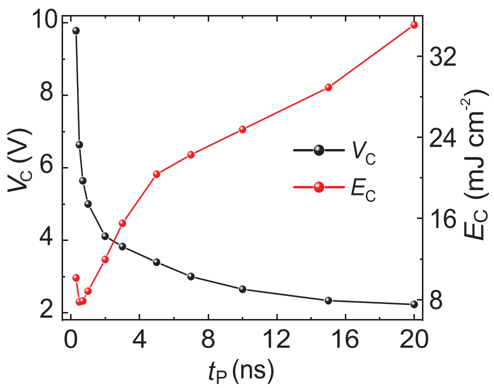

Figure 13. Threshold switching voltage (black dots, left scale) and energy density (red dots, right scale) as a function of the pulse length at a constant in-plane magnetic field of 100 mT. The measurements were performed on a GdFeCo device with the same composition and geometry as that in Figure 10. Reproduced under the terms of the CC-BY license.[57] Copyright 2021, Springer Nature.

findings were reproduced only under two conditions: 1) the SOTs exerted on the TM sublattice are stronger than on the RE sublattice; 2) the antiferromagnetic exchange interaction between the two sublattices is weak. The combination of these two points leads to a master-agent dynamics by which the SOTs switch the TM sublattice, which in turn drags the reversal of the RE magnetization. The speed of the latter is determined by the strength C_{ex} of the antiferromagnetic coupling. The simulated switching dynamics transitions from type I to type III in a narrow range of C_{ex} independently of the applied magnetic field, STT, field-like SOT, DMI, thermal fluctuations, defects, and random spatial variations of the magnetic quantities (see Figure 16 and ref. [58]). These parameters play a secondary role and cannot explain the asynchronous dynamics. Point (1) supports the idea that SOTs interact predominantly with the TM magnetic moments because of the different localization of 4f and 3d electrons.[70,143,152,153] Point (2), instead, challenges the traditional assumption of rigid antiferromagnetic coupling in RE-TM ferrimagnets at timescales exceeding the ps regime. This point is supported by the experimental evidence of a ns-long transient ferromagnetic state.

The low value of C_{ex} was linked to microstructure of ferrimagnetic alloys and its metastable nature. The comparison between multiple measurements in distinct devices suggests the existence of a correlation between the sample age and the strength of C_{ex} because the dynamics progressively transitioned from type I to type III in a period of one year.[58] As discussed in Section 2, GdFeCo alloys host Gd and Fe clusters of nm dimensions that tend to become smaller and more homogeneous with time. The formation of Gd-rich and Fe-rich clusters reduces the intersublattice coupling relative to the homogeneous phase by limiting the number of direct Fe–Gd interactions.[154] This reduction may be further enhanced by the sperimagnetic order typical of RE-TM ferrimagnets,[100,102] which leads to a distribution of interatomic exchange interactions. However, the negative mixing enthalpy of TM and RE atoms drives the intermixing of the two atomic species. This atomic relaxation affects C_{ex} and, ultimately, the type of dynamics during the SOT-induced switching.

5.3. Discussion of the Asynchronous Dynamics

The asynchronous sublattice magnetization dynamics is reminiscent of all-optical switching observed in GdFeCo alloys.[88,155–157] Yet, the measurements reported in ref. [58] show that the decoupling of the RE and TM magnetization dynamics is a general feature of RE-TM alloys that extends well beyond the ultrafast temporal regime of all-optical switching and involves also SOTs. In addition, there exist important differences between all-optical and SOT switching: the primary cause, that is, Joule heating versus SOTs; the absence of a spatially-coherent dynamics versus the domain-wall-driven reversal; the transient ferromagnetic state as a prerequisite and unique reversal path versus the dynamics of types II and III; the longitudinal versus the transverse magnetization dynamics.

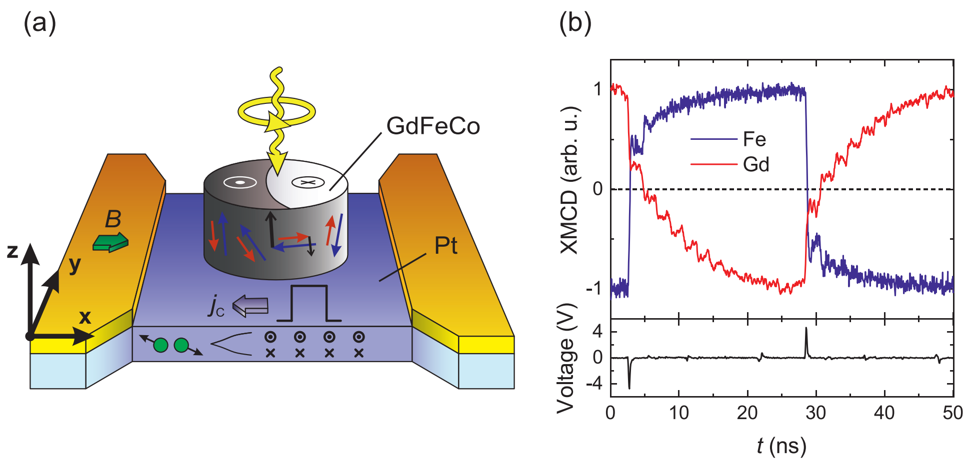

Figure 14. a) Schematic of the current-pump, X-ray-probe detection of the switching of a 1-µm-wide GdFeCo(15 nm) dot on a Pt(5 nm) current line. The samples were deposited on a Si_3N_4 membrane transparent to X-rays. b) Time-dependence of the spatially-averaged XMCD signal measured while applying bipolar electric pulses with 200 ps duration and 4.8 V amplitude to a $Gd_{31}Fe_{62}Co_7$(15 nm) dot. The bottom panel shows the amplitude and duration of the voltage pulses. Adapted under the terms of the CC-BY license.[58] Copyright 2022, Springer Nature.

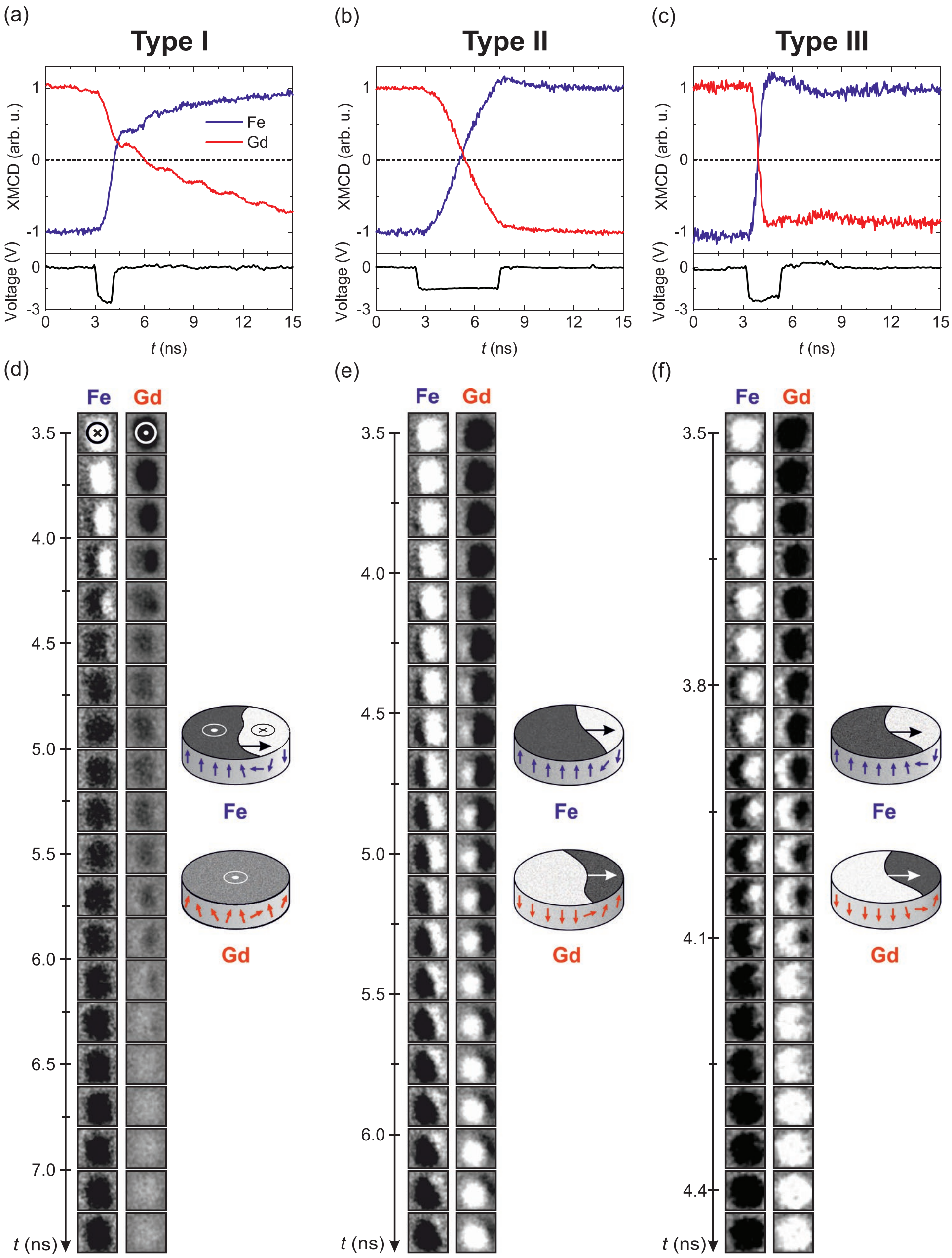

Figure 15. a–c) Time dependence of the spatially-averaged XMCD contrast at the Fe and Gd edges for three distinct devices, whose respective composition is $Gd_{31}Fe_{62}Co_7$ (15 nm), $Gd_{30}Fe_{63}Co_7$ (15 nm), and $Gd_{29}Fe_{64}Co_7$ (15 nm). d–f) Corresponding spatially-resolved snapshots of the dynamics and schematics showing the orientation of the magnetic moments of Fe and Gd during the switching and the domain wall profile. Reproduced under the terms of the CC-BY license.[58] Copyright 2022, Springer Nature.

This comparison demonstrates that the ns-long non-equilibrium ferromagnetic state cannot be explained by the thermal collapse of the longitudinal magnetization of the TM sublattice, as in all-optical switching. Such a long-lived transient state can only be rationalized by assuming uneven transfer of angular momentum from the electric current to the TM and RE sublattices and a relatively weak coupling among them, in agreement with the micromagnetic simulations.

We also exclude that the compensation of the magnetization and/or angular momentum play a role in the asynchronous switching. As discussed before, the magnetization compensation point is not fundamentally relevant to the dynamics and switching of ferrimagnets because it does not alter the amount of angular momentum injected from Pt into GdFeCo or TbCo nor the strength of SOTs. Indeed, Tb-dominated and Co-dominated TbCo samples manifest similar dynamics. Moreover, the compensation of the angular momentum was not crucial in these experiments. First, T_A was close to or below room temperature in all GdFeCo samples. Second, although the net angular momentum strongly influences the speed of domain

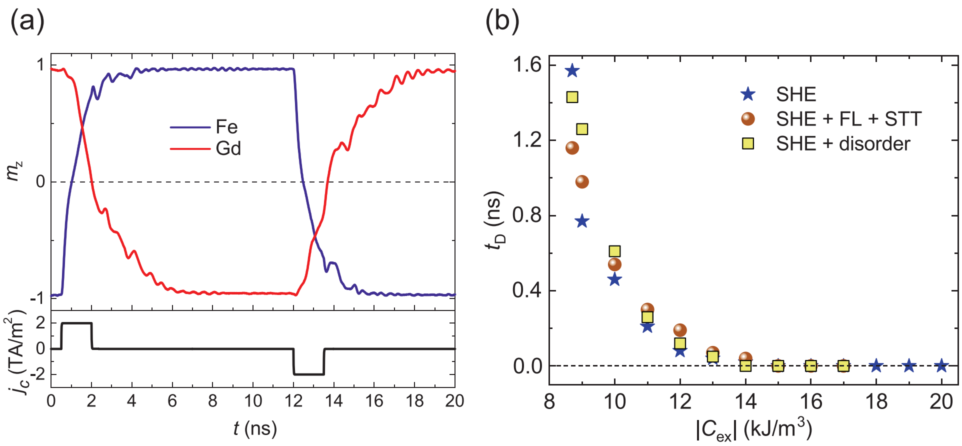

Figure 16. a) Time dependence of the simulated average component m_z of $\mathbf{M}_{Fe}$ and $\mathbf{M}_{Gd}$ in a GdFeCo (15 nm) device when $C_{ex} = -6.8$ kJ m^{-3}. b) Delay $t_D = t_{Fe} - t_{Gd}$ between the times at which the m_z components of $\mathbf{M}_{Fe}$ and $\mathbf{M}_{Gd}$ cross zero as a function of the antiferromagnetic exchange energy density $|C_{ex}|$. The simulations assume effective spin Hall angles $\theta_{SH}^{TM} = 0.21$, $\theta_{SH}^{RE} = 0.07$ and dampinglike SOT (stars), field like torque and spin transfer torque (circles), thermal fluctuations and grains of 10 nm size with 10% random variations of the magnetic anisotropy (squares). Adapted under the terms of the CC-BY license.[58] Copyright 2022, Springer Nature.

walls, it does not determine the type of dynamics, which is solely determined by the strength of the antiferromagnetic exchange interaction. Because C_{ex} may depend on the stoichiometry but not on the net angular momentum,[73,75] the variation of the latter close to its compensation point cannot explain the asynchronous dynamics.

In conclusion, these measurements reveal that the RE and TM sublattices of ferrimagnetic alloys are not necessarily rigidly coupled and react differently to SOTs despite the high domain wall speed typical of ferrimagnets. This finding provides evidence of the asymmetric action of SOTs on the two sublattices, which was a long-standing open point for ferrimagnets. This study also complements the time-resolved Hall measurements presented in the previous section by providing a different perspective on the ferrimagnetic dynamics induced by SOTs. It supports the identification of t_0 with the incubation time that precedes the reversal of an edge domain, and confirms that the transition time Δt can be associated to the motion of a domain wall across the dot due to the concerted action of the dampinglike SOT and DMI, as previously observed in ferromagnets.[54]

6. Conclusion and Outlook

RE-TM ferrimagnets have attracted considerable attention because of outstanding properties that make them viable candidates for spintronic applications: the small magnetization and stray field, the bulk anisotropy and DMI, the possibility to engineer the sample composition and structure, and, above all, the fast current-induced dynamics. The measurements presented in Sections 4 and 5 provide a comprehensive picture of this dynamics. In particular, it has been possible to: 1) identify the distinct phases and timescales that characterize the magnetization switching and the underlying physical processes (domain nucleation and domain wall motion); 2) understand their dependence on the driving parameters (electric current and magnetic field); 3) reveal the intrinsic stochastic nature of switching; 4) highlight the asymmetric SOTs and ensuing master-agent behavior of the RE and TM sublattices; and 5) describe the asynchronous switching of the RE and TM magnetizations as a function of the antiferromagnetic coupling strength and its dependence on the alloy structure. These findings have fundamental and practical implications that are not limited to ferrimagnetic materials. Points (1)–(3) are generally applicable to ferromagnets and, to some extent, also to true antiferromagnets because the physics of SOTs is common to all magnetic materials and Joule heating is an inevitable companion of electric currents. Point (4) may appear specific to RE-TM ferrimagnets, but is in fact doubly relevant. It is instrumental in understanding the exchange of angular momentum in systems involving different magnetic bands or orbitals, which, beside RE-TM ferrimagnets, include compounds such as Heusler alloys (MnGa, MnGe), garnets (TbIG, GdIG), and antiferromagnets (CuMnAs, Mn_2Au). In addition, it underscores the often overlooked complexity of multi-sublattice magnetic systems, which can react distinctly to external stimuli.

In this regard, it is instructive to recall the different participation of the RE and TM sublattices in magnetotransport. The anomalous Hall effect and the spin polarization of the conduction electrons are dominated by the TM atoms,[152,158–160] but the RE elements can generate non-negligible SOTs thanks to the sizable spin-orbit coupling of the 5d states at the Fermi level.[161–164] Moreover, the RE and TM magnetizations interact differently with spin currents. This scenario is supported by the element-resolved switching measurements presented in Section 5 and by additional evidence. First, the sign of the spin Hall magnetoresistance of ferrimagnets does not vary across either the magnetic or angular momentum compensation point and is the same as in bilayers composed of a heavy metal and a ferromagnet.[153] This suggests that the interfacial spin accumulation interacts preferentially with the TM sublattice. Second, the dephasing of spin currents polarized transverse to the net magnetization is mitigated in ferrimagnets relative to ferromagnets but appears to be dominated by the exchange coupling between the injected spins and the TM moments.[143,165] This picture agrees with the sublattice-dependent SOTs evidenced by the switching experiments and micromagnetic simulations.[58] The overall picture that emerges from such considerations is that RE elements actively participate in transport effects through their 5d orbitals, but that the coupling between nonequilibrium spins and the RE magnetization is weaker than in ferromagnets, likely because the RE magnetic moments are localized in the 4f orbitals.

In this context, the observation of so-called self-torques in single layer RE-TM alloys raises interesting questions.[96,104,166–168] The generation of self-torques in systems without an external source of spin or orbital current[31] may entail an unusual mechanism by which first the RE element realizes the charge-to-spin conversion, then the SOTs acting on the TM sublattice are transferred back to the RE magnetization by the antiferromagnetic coupling. In the future, more efforts could be dedicated to explore this possibility and, more generally, to unravel the physics of self-torques as well as of the bulk DMI in these systems.[103]

Taking advantage of the rapidity and efficiency of magnetization switching in RE-TM ferrimagnets also requires tackling open problems. RE-TM compounds are physically and chemically metastable,[76] are sensitive to temperature variations, and provide a modest tunneling magnetoresistance for integration into magnetic tunnel junction devices.[169–171] These drawbacks pose serious technological challenges. However, ferrimagnetic order is by no means restricted to RE-TM compounds, and other materials such as garnets and Heusler alloys provide interesting opportunities for device integration. For example, all-optical switching has been demonstrated in MnRuGa,[172] and ferrimagnetic Heusler alloys could in principle enable tunneling magnetoresistance.[173] Moreover, efficient current-induced reversal and fast domain wall motion have been observed in TmIG[174–176] and MnN.[177] The fast dynamics found in other RE-free compounds is not surprising because it is rooted in the common underlying ferrimagnetic order. Therefore, the favorable energy scaling presented in Figures 1 and 13 is expected to apply to other ferrimagnets, leading to fast and efficient ferrimagnet-based applications.

Acknowledgements

This research was partially supported by the Swiss National Science Foundation (Grant No. 200020-200465).

Open access funding provided by Eidgenossische Technische Hochschule Zurich.

Conflict of Interest

The authors declare no conflict of interest.

Keywords

antiferromagnets, ferrimagnets, magnetization switching, spin-orbit torques

Received: July 23, 2022
Revised: September 5, 2022
Published online:

[1] L. Berger, *J. Appl. Phy.* **1978**, *49*, 2156.
[2] J. Slonczewski, *J. Magn. Magn. Mater.* **1996**, *159*, L1.
[3] L. Berger, *Phys. Rev. B* **1996**, *54*, 9353.
[4] D. Ralph, M. Stiles, *J. Magn. Magn. Mater.* **2008**, *320*, 1190.
[5] A. Brataas, A. D. Kent, H. Ohno, *Nat. Mater.* **2012**, *11*, 372.
[6] A. D. Kent, D. C. Worledge, *Nat. Nanotechnol.* **2015**, *10*, 187.
[7] M. D. Stiles, J. Miltat, in *Spin Dynamics in Confined Magnetic Structures III*, Springer Berlin Heidelberg, **2006**, pp. 225–308.
[8] I. M. Miron, G. Gaudin, S. Auffret, B. Rodmacq, A. Schuhl, S. Pizzini, J. Vogel, P. Gambardella, *Nat. Mater.* **2010**, *9*, 230.
[9] I. M. Miron, K. Garello, G. Gaudin, P.-J. Zermatten, M. V. Costache, S. Auffret, S. Bandiera, B. Rodmacq, A. Schuhl, P. Gambardella, *Nature* **2011**, *476*, 189.
[10] L. Liu, C.-F. Pai, Y. Li, H. W. Tseng, D. C. Ralph, R. A. Buhrman, *Science* **2012**, *336*, 555.
[11] K. Garello, I. M. Miron, C. O. Avci, F. Freimuth, Y. Mokrousov, S. Blügel, S. Auffret, O. Boulle, G. Gaudin, P. Gambardella, *Nat. Nanotechnol.* **2013**, *8*, 587.
[12] J. Kim, J. Sinha, M. Hayashi, M. Yamanouchi, S. Fukami, T. Suzuki, S. Mitani, H. Ohno, *Nat. Mater.* **2013**, *12*, 240.
[13] A. Manchon, J. Železný, I. M. Miron, T. Jungwirth, J. Sinova, A. Thiaville, K. Garello, P. Gambardella, *Rev. Mod. Phys.* **2019**, *91*, 035004.
[14] C.-F. Pai, M.-H. Nguyen, C. Belvin, L. H. Vilela-Leão, D. C. Ralph, R. A. Buhrman, *Appl. Phys. Lett.* **2014**, *104*, 082407.
[15] J. Sinova, S. O. Valenzuela, J. Wunderlich, C. H. Back, T. Jungwirth, *Rev. Mod. Phys.* **2015**, *87*, 1213.
[16] A. Manchon, S. Zhang, *Phys. Rev. B* **2008**, *78*, 212405.
[17] P. Gambardella, I. M. Miron, *Philos. Trans. R. Soc., A* **2011**, *369*, 3175.
[18] J. C. R. Sánchez, L. Vila, G. Desfonds, S. Gambarelli, J. P. Attané, J. M. De Teresa, C. Magén, A. Fert, *Nat. Commun.* **2013**, *4*, 2944.
[19] P. M. Haney, H.-W. Lee, K.-J. Lee, A. Manchon, M. D. Stiles, *Phys. Rev. B* **2013**, *88*, 214417.
[20] F. Freimuth, S. Blügel, Y. Mokrousov, *Phys. Rev. B* **2014**, *90*, 174423.
[21] X. Fan, H. Celik, J. Wu, C. Ni, K.-J. Lee, V. O. Lorenz, J. Q. Xiao, *Nat. Commun.* **2014**, *5*, 3042.
[22] V. P. Amin, M. D. Stiles, *Phys. Rev. B* **2016**, *94*, 104419.
[23] Y. Ou, C. F. Pai, S. Shi, D. C. Ralph, R. A. Buhrman, *Phys. Rev. B* **2016**, *94*, 140414.
[24] A. M. Humphries, T. Wang, E. R. J. Edwards, S. R. Allen, J. M. Shaw, H. T. Nembach, J. Q. Xiao, T. J. Silva, X. Fan, *Nat. Commun.* **2017**, *8*, 911.
[25] A. Ghosh, K. Garello, C. O. Avci, M. Gabureac, P. Gambardella, *Phys. Rev. Appl.* **2017**, *7*, 014004.
[26] V. P. Amin, J. Zemen, M. D. Stiles, *Phys. Rev. Lett.* **2018**, *121*, 136805.
[27] C. Safranski, E. A. Montoya, I. N. Krivorotov, *Nat. Nanotechnol.* **2019**, *14*, 27.
[28] D. Go, D. Jo, C. Kim, H. W. Lee, *Phys. Rev. Lett.* **2018**, *121*, 86602.
[29] D. Go, H.-W. Lee, *Phys. Rev. Res.* **2020**, *2*, 013177.
[30] D. Lee, D. Go, H.-J. Park, W. Jeong, H.-W. Ko, D. Yun, D. Jo, S. Lee, G. Go, J. H. Oh, K.-J. Kim, B.-G. Park, B.-C. Min, H. C. Koo, H.-W. Lee, O. Lee, K.-J. Lee, *Nat. Commun.* **2021**, *12*, 6710.
[31] G. Sala, P. Gambardella, *Phys. Rev. Res.* **2022**, *4*, 033037.
[32] A. R. Mellnik, J. S. Lee, A. Richardella, J. L. Grab, P. J. Mintun, M. H. Fischer, A. Vaezi, A. Manchon, E.-A. Kim, N. Samarth, D. C. Ralph, *Nature* **2014**, *511*, 449.
[33] Y. Fan, P. Upadhyaya, X. Kou, M. Lang, S. Takei, Z. Wang, J. Tang, L. He, L.-T. Chang, M. Montazeri, G. Yu, W. Jiang, T. Nie, R. N. Schwartz, Y. Tserkovnyak, K. L. Wang, *Nat. Mater.* **2014**, *13*, 699.
[34] Y. Wang, P. Deorani, K. Banerjee, N. Koirala, M. Brahlek, S. Oh, H. Yang, *Phys. Rev. Lett.* **2015**, *114*, 257202.

[35] P. Li, J. Kally, S. S.-L. Zhang, T. Pillsbury, J. Ding, G. Csaba, J. Ding, J. S. Jiang, Y. Liu, R. Sinclair, C. Bi, A. DeMann, G. Rimal, W. Zhang, S. B. Field, J. Tang, W. Wang, O. G. Heinonen, V. Novosad, A. Hoffmann, N. Samarth, M. Wu, *Sci. Adv.* **2019**, *5*, 8.
[36] F. Binda, C. O. Avci, S. F. Alvarado, P. Noël, C.-H. Lambert, P. Gambardella, *Phys. Rev. B* **2021**, *103*, 224428.
[37] K.-s. Ryu, L. Thomas, S.-h. Yang, S. Parkin, *Nat. Nanotechnol.* **2013**, *8*, 527.
[38] S. Emori, U. Bauer, S.-M. Ahn, E. Martinez, G. S. D. Beach, *Nat. Mater.* **2013**, *12*, 611.
[39] J. Torrejon, J. Kim, J. Sinha, S. Mitani, M. Hayashi, M. Yamanouchi, H. Ohno, *Nat. Commun.* **2014**, *5*, 4655.
[40] S. Woo, K. Litzius, B. Krüger, M.-Y. Im, L. Caretta, K. Richter, M. Mann, A. Krone, R. M. Reeve, M. Weigand, P. Agrawal, I. Lemesh, M.-A. Mawass, P. Fischer, M. Kläui, G. S. D. Beach, *Nat. Mater.* **2016**, *15*, 501.
[41] F. Büttner, I. Lemesh, M. Schneider, B. Pfau, C. M. Günther, P. Hessing, J. Geilhufe, L. Caretta, D. Engel, B. Krüger, J. Viefhaus, S. Eisebitt, G. S. D. Beach, *Nat. Nanotechnol.* **2017**, *12*, 1040.
[42] S. Woo, K. M. Song, X. Zhang, M. Ezawa, Y. Zhou, X. Liu, M. Weigand, S. Finizio, J. Raabe, M.-c. Park, K.-y. Lee, J. W. Choi, B.-c. Min, H. C. Koo, J. Chang, *Nat. Electron.* **2018**, *1*, 288.
[43] S. Vélez, S. Ruiz-Gómez, J. Schaab, E. Gradauskaite, M. S. Wörnle, P. Welter, B. J. Jacot, C. L. Degen, M. Trassin, M. Fiebig, P. Gambardella, *Nat. Nanotechnol.* **2022**, *17*, 834.
[44] Z. Luo, A. Hrabec, T. P. Dao, G. Sala, S. Finizio, J. Feng, S. Mayr, J. Raabe, P. Gambardella, L. J. Heyderman, *Nature* **2020**, *579*, 214.
[45] M. Cubukcu, O. Boulle, M. Drouard, K. Garello, C. Onur Avci, I. Mihai Miron, J. Langer, B. Ocker, P. Gambardella, G. Gaudin, *Appl. Phys. Lett.* **2014**, *104*, 042406.
[46] S. V. Aradhya, G. E. Rowlands, J. Oh, D. C. Ralph, R. A. Buhrman, *Nano Lett.* **2016**, *16*, 5987.
[47] S. Fukami, T. Anekawa, C. Zhang, H. Ohno, *Nat. Nanotechnol.* **2016**, *11*, 621.
[48] M. Wang, W. Cai, D. Zhu, Z. Wang, J. Kan, Z. Zhao, K. Cao, Z. Wang, Y. Zhang, T. Zhang, C. Park, J.-P. Wang, A. Fert, W. Zhao, *Nat. Electron.* **2018**, *1*, 582.
[49] E. Grimaldi, V. Krizakova, G. Sala, F. Yasin, S. Couet, G. Sankar Kar, K. Garello, P. Gambardella, *Nat. Nanotechnol.* **2020**, *15*, 111.
[50] V. Krizakova, K. Garello, E. Grimaldi, G. S. Kar, P. Gambardella, *Appl. Phys. Lett.* **2020**, *116*, 232406.
[51] V. Krizakova, E. Grimaldi, K. Garello, G. Sala, S. Couet, G. S. Kar, P. Gambardella, *Phys. Rev. Appl.* **2021**, *15*, 054055.
[52] Y. Wu, K. Garello, W. Kim, M. Gupta, M. Perumkunnil, V. Kateel, S. Couet, R. Carpenter, S. Rao, S. Van Beek, K. Vudya Sethu, F. Yasin, D. Crotti, G. Kar, *Phys. Rev. Appl.* **2021**, *15*, 064015.
[53] V. Krizakova, M. Perumkunnil, S. Couet, P. Gambardella, K. Garello, *J. Magn. Magn. Mater.* **2022**, *562*, 169692.
[54] M. Baumgartner, K. Garello, J. Mendil, C. O. Avci, E. Grimaldi, C. Murer, J. Feng, M. Gabureac, C. Stamm, Y. Acremann, S. Finizio, S. Wintz, J. Raabe, P. Gambardella, *Nat. Nanotechnol.* **2017**, *12*, 980.
[55] K. Garello, C. O. Avci, I. M. Miron, M. Baumgartner, A. Ghosh, S. Auffret, O. Boulle, G. Gaudin, P. Gambardella, *Appl. Phys. Lett.* **2014**, *105*, 212402.
[56] M. Cubukcu, O. Boulle, N. Mikuszeit, C. Hamelin, T. Bracher, N. Lamard, M.-C. C. Cyrille, L. Buda-Prejbeanu, K. Garello, I. M. Miron, O. Klein, G. De Loubens, V. V. Naletov, J. Langer, B. Ocker, P. Gambardella, G. Gaudin, *IEEE Trans. Magn.* **2018**, *54*, 81.
[57] G. Sala, V. Krizakova, E. Grimaldi, C.-H. Lambert, T. Devolder, P. Gambardella, *Nat. Commun.* **2021**, *12*, 656.
[58] G. Sala, C.-h. Lambert, S. Finizio, V. Raposo, V. Krizakova, G. Krishnaswamy, M. Weigand, J. Raabe, M. D. Rossell, E. Martinez, P. Gambardella, *Nat. Mater.* **2022**, *21*, 640.
[59] K. Cai, Z. Zhu, J. M. Lee, R. Mishra, L. Ren, S. D. Pollard, P. He, G. Liang, K. L. Teo, H. Yang, *Nat. Electron.* **2020**, *3*, 37.
[60] D. Bedau, H. Liu, J. Z. Sun, J. A. Katine, E. E. Fullerton, S. Mangin, A. D. Kent, *Appl. Phys. Lett.* **2010**, *97*, 262502.
[61] H. Liu, D. Bedau, J. Z. Sun, S. Mangin, E. E. Fullerton, J. A. Katine, A. D. Kent, *J. Magn. Magn. Mater.* **2014**, *358–359*, 233.
[62] K. K. Vudya Sethu, S. Ghosh, S. Couet, J. Swerts, B. Sorée, J. De Boeck, G. S. Kar, K. Garello, *Phys. Rev. Appl.* **2021**, *16*, 064009.
[63] K.-J. Kim, S. K. Kim, Y. Hirata, S.-h. Oh, T. Tono, D.-H. Kim, T. Okuno, W. S. Ham, S. Kim, G. Go, Y. Tserkovnyak, A. Tsukamoto, T. Moriyama, K.-j. Lee, T. Ono, *Nat. Mater.* **2017**, *16*, 1187.
[64] L. Caretta, M. Mann, F. Büttner, K. Ueda, B. Pfau, C. M. Günther, P. Hessing, A. Churikova, C. Klose, M. Schneider, D. Engel, C. Marcus, D. Bono, K. Bagschik, S. Eisebitt, G. S. D. Beach, *Nat. Nanotechnol.* **2018**, *13*, 1154.
[65] R. Bläsing, T. Ma, S.-H. Yang, C. Garg, F. K. Dejene, A. T. N'Diaye, G. Chen, K. Liu, S. S. P. Parkin, *Nat. Commun.* **2018**, *9*, 4984.
[66] J. Finley, L. Liu, *Appl. Phys. Lett.* **2020**, *116*, 110501.
[67] S. K. Kim, G. S. D. Beach, K.-J. Lee, T. Ono, T. Rasing, H. Yang, *Nat. Mater.* **2022**, *21*, 24.
[68] M. S. Brooks, O. Eriksson, B. Johansson, *J. Phys.: Condens. Matter* **1989**, *1*, 5861.
[69] M. S. Brooks, L. Nordstrom, B. Johansson, *J. Phys.: Condens. Matter* **1991**, *3*, 2357.
[70] H. Tanaka, S. Takayama, T. Fujiwara, *Phys. Rev. B* **1992**, *46*, 7390.
[71] M. S. S. Brooks, in *Mathematisk-Fysiske Meddelelser* (Eds: D. F. McMorrow, J. Jensen, H. M. Rønnow), The Royal Danish Academy of Sciences and Letters, København **1997**, pp. 291–314.
[72] M. Richter, *J. Phys. D: Appl. Phys.* **1998**, *31*, 1017.
[73] N. H. Duc, *Adv. Magn. Magn. Mater.* **2014**, *1*, 9.
[74] I. A. Campbell, *J. Phys. F: Met. Phys.* **1972**, *2*, 3.
[75] K. H. J. Buschow, *Rep. Prog. Phys.* **1977**, *40*, 1179.
[76] P. Hansen, *Handb. Magn. Mater.* **1991**, *6*, 289.
[77] Y. Hirata, D.-H. Kim, T. Okuno, T. Nishimura, D.-Y. Kim, Y. Futakawa, H. Yoshikawa, A. Tsukamoto, K.-j. Kim, S.-b. Choe, T. Ono, *Phys. Rev. B* **2018**, *97*, 220403.
[78] C. D. Stanciu, A. V. Kimel, F. Hansteen, A. Tsukamoto, A. Itoh, A. Kirilyuk, T. Rasing, *Phys. Rev. B* **2006**, *73*, 220402.
[79] M. Binder, A. Weber, O. Mosendz, G. Woltersdorf, M. Izquierdo, I. Neudecker, J. R. Dahn, T. D. Hatchard, J.-U. Thiele, C. H. Back, M. R. Scheinfein, *Phys. Rev. B* **2006**, *74*, 134404.
[80] D.-H. Kim, T. Okuno, S. K. Kim, S.-H. Oh, T. Nishimura, Y. Hirata, Y. Futakawa, H. Yoshikawa, A. Tsukamoto, Y. Tserkovnyak, Y. Shiota, T. Moriyama, K.-J. Kim, K.-J. Lee, T. Ono, *Phys. Rev. Lett.* **2019**, *122*, 127203.
[81] R. W. Cochrane, R. Harris, M. J. Zuckermann, *Phys. Rep.* **1978**, *1*, 1.
[82] T. Mizoguchi, G. S. CargillIII, *J. Appl. Phys.* **1979**, *50*, 3570.
[83] K. H. J. Buschow, in *Handbook on the Physics' and Chemistry of Rare Earths*, (Eds: K. Gschneidner, L. Eyring), Chapter 52, Elsevier Science, Amsterdam, Netherlands **1984**, pp. 265–443.
[84] B. Hebler, A. Hassdenteufel, P. Reinhardt, H. Karl, M. Albrecht, *Front. Mater.* **2016**, *3*, 1.
[85] M. H. Kryder, *J. Appl. Phys.* **1985**, *57*, 3913.
[86] S. Tsunashima, *J. Phys. D: Appl. Phys.* **2001**, *34*, R87.
[87] F. Radu, J. Sánchez-Barriga, in *Novel Magnetic Nanostructures*, Elsevier, Amsterdam, Netherlands **2018**, pp. 267–331.
[88] A. V. Kimel, M. Li, *Nat. Rev. Mater.* **2019**, *4*, 189.
[89] Z. G. Li, D. J. Smith, E. E. Marinero, *J. Appl. Phys.* **1991**, *69*, 6590.
[90] Y. Mimura, N. Imamura, T. Kobayashi, A. Okada, Y. Kushiro, *J. Appl. Phys.* **1978**, *49*, 1208.
[91] T. Gao, X. Xu, S. Zhou, J. Li, A.-L. Xia, B.-S. Han, *J. Magn. Magn. Mater.* **2006**, *306*, 324.
[92] A. Frisk, F. Magnus, S. George, U. B. Arnalds, G. Andersson, *J. Phys. D: Appl. Phys.* **2016**, *49*, 035005.

[93] C. E. Graves, A. H. Reid, T. Wang, B. Wu, S. De Jong, K. Vahaplar, I. Radu, D. P. Bernstein, M. Messerschmidt, L. Müller, R. Coffee, M. Bionta, S. W. Epp, R. Hartmann, N. Kimmel, G. Hauser, A. Hartmann, P. Holl, H. Gorke, J. H. Mentink, A. Tsukamoto, A. Fognini, J. J. Turner, W. F. Schlotter, D. Rolles, H. Soltau, L. Strüder, Y. Acremann, A. V. Kimel, A. Kirilyuk, et al., *Nat. Mater.* **2013**, *12*, 293.
[94] T.-M. Liu, T. Wang, A. H. Reid, M. Savoini, X. Wu, B. Koene, P. Granitzka, C. E. Graves, D. J. Higley, Z. Chen, G. Razinskas, M. Hantschmann, A. Scherz, J. Stöhr, A. Tsukamoto, B. Hecht, A. V. Kimel, A. Kirilyuk, T. Rasing, H. A. Dürr, *Nano Lett.* **2015**, *15*, 6862.
[95] E. Kirk, C. Bull, S. Finizio, H. Sepehri-Amin, S. Wintz, A. K. Suszka, N. S. Bingham, P. Warnicke, K. Hono, P. W. Nutter, J. Raabe, G. Hrkac, T. Thomson, L. J. Heyderman, *Phys. Rev. Mater.* **2020**, *4*, 074403.
[96] S. Krishnia, E. Haltz, L. Berges, L. Aballe, M. Foerster, L. Bocher, R. Weil, A. Thiaville, J. Sampaio, A. Mougin, *Phys. Rev. Appl.* **2021**, *10*, 024040.
[97] P. Bernstein, C. Gueugnon, *J. Appl. Phys.* **1984**, *55*, 1760.
[98] B. Konar, J. Kim, I.-H. Jung, *J. Phase Equilib. Diffus.* **2017**, *38*, 509.
[99] J. M. Coey, *J. Appl. Phys.* **1978**, *49*, 1646.
[100] R. C. Taylor, A. Gangulee, *Phys. Rev. B* **1980**, *22*, 1320.
[101] T. Danh, N. Duc, N. Thuy, *J. Magn. Magn. Mater.* **1998**, *185*, 105.
[102] J. Park, Y. Hirata, J.-h. Kang, S. Lee, S. Kim, C. Van Phuoc, J.-r. Jeong, J. Park, S.-y. Park, Y. Jo, A. Tsukamoto, T. Ono, S. K. Kim, K.-j. Kim, *Phys. Rev. B* **2021**, *103*, 014421.
[103] D.-H. Kim, M. Haruta, H.-W. Ko, G. Go, H.-J. Park, T. Nishimura, D.-Y. D.-H. Kim, T. Okuno, Y. Hirata, Y. Futakawa, H. Yoshikawa, W. Ham, S. Kim, H. Kurata, A. Tsukamoto, Y. Shiota, T. Moriyama, S.-B. Choe, K.-J. Lee, T. Ono, *Nat. Mater.* **2019**, *18*, 685.
[104] Z. Zheng, Y. Zhang, V. Lopez-Dominguez, L. Sánchez-Tejerina, J. Shi, X. Feng, L. Chen, Z. Wang, Z. Zhang, K. Zhang, B. Hong, Y. Xu, Y. Zhang, M. Carpentieri, A. Fert, G. Finocchio, W. Zhao, P. Khalili Amiri, *Nat. Commun.* **2021**, *12*, 4555.
[105] T. Kobayashi, H. Hayashi, Y. Fujiwara, S. Shiomi, *IEEE Trans. Magn.* **2005**, *41*, 2848.
[106] S.-G. Je, J.-C. Rojas-Sánchez, T. H. Pham, P. Vallobra, G. Malinowski, D. Lacour, T. Fache, M.-C. Cyrille, D.-Y. Kim, S.-B. Choe, M. Belmeguenai, M. Hehn, S. Mangin, G. Gaudin, O. Boulle, *Appl. Phys. Lett.* **2018**, *112*, 062401.
[107] S. A. Siddiqui, J. Han, J. T. Finley, C. A. Ross, L. Liu, *Phys. Rev. Lett.* **2018**, *121*, 057701.
[108] S. H. Oh, S. K. Kim, D. K. Lee, G. Go, K. J. Kim, T. Ono, Y. Tserkovnyak, K. J. Lee, *Phys. Rev. B* **2017**, *96*, 100407.
[109] S.-H. Oh, K.-J. Lee, *J. Magn.* **2018**, *23*, 196.
[110] T. Okuno, S. K. Kim, T. Moriyama, D.-H. Kim, H. Mizuno, T. Ikebuchi, Y. Hirata, H. Yoshikawa, A. Tsukamoto, K.-J. Kim, Y. Shiota, K.-J. Lee, T. Ono, *Appl. Phys. Express* **2019**, *12*, 093001.
[111] A. Kamra, R. E. Troncoso, W. Belzig, A. Brataas, *Phys. Rev. B* **2018**, *98*, 184402.
[112] T. L. Gilbert, *IEEE Trans. Magn.* **2004**, *40*, 3443.
[113] A. Mekonnen, M. Cormier, A. V. Kimel, A. Kirilyuk, A. Hrabec, L. Ranno, T. Rasing, *Phys. Rev. Lett.* **2011**, *107*, 117202.
[114] K. Ueda, M. Mann, C.-f. Pai, A.-j. Tan, G. S. D. Beach, *Appl. Phys. Lett.* **2016**, *109*, 232403.
[115] J. Finley, L. Liu, *Phys. Rev. Appl.* **2016**, *6*, 054001.
[116] W. Seung Ham, S. Kim, D.-H. Kim, K.-j. Kim, T. Okuno, H. Yoshikawa, A. Tsukamoto, T. Moriyama, T. Ono, *Appl. Phys. Lett.* **2017**, *110*, 242405.
[117] N. Roschewsky, C.-h. Lambert, S. Salahuddin, *Phys. Rev. B* **2017**, *96*, 064406.
[118] K. Ueda, M. Mann, P. W. P. de Brouwer, D. Bono, G. S. D. Beach, *Phys. Rev. B* **2017**, *96*, 064410.
[119] R. Mishra, J. Yu, X. Qiu, M. Motapothula, T. Venkatesan, H. Yang, *Phys. Rev. Lett.* **2017**, *118*, 167201.
[120] H. Xue, S. Chen, D. Wu, W. Zhu, Y. Zhang, C. Duan, J. Chen, Q. Jin, Z. Zhang, *Adv. Electron. Mater.* **2019**, *5*, 1900014.
[121] I. M. Miron, T. Moore, H. Szambolics, L. D. Buda-Prejbeanu, S. Auffret, B. Rodmacq, S. Pizzini, J. Vogel, M. Bonfim, A. Schuhl, G. Gaudin, *Nat. Mater.* **2011**, *10*, 419.
[122] A. Thiaville, S. Rohart, É. Jué, V. Cros, A. Fert, *Europhys. Lett.* **2012**, *100*, 57002.
[123] A. V. Khvalkovskiy, V. Cros, D. Apalkov, V. Nikitin, M. Krounbi, K. A. Zvezdin, A. Anane, J. Grollier, A. Fert, *Phys. Rev. B* **2013**, *87*, 020402.
[124] S. Emori, E. Martinez, K.-J. Lee, H.-W. Lee, U. Bauer, S.-M. Ahn, P. Agrawal, D. C. Bono, G. S. D. Beach, *Phys. Rev. B* **2014**, *90*, 184427.
[125] S. S. P. Parkin, M. Hayashi, L. Thomas, *Science* **2008**, *320*, 190.
[126] E. Haltz, S. Krishnia, L. Berges, A. Mougin, J. Sampaio, *Phys. Rev. B* **2021**, *103*, 014444.
[127] G. S. D. Beach, C. Nistor, C. Knutson, M. Tsoi, J. L. Erskine, *Nat. Mater.* **2005**, *4*, 741.
[128] A. Mougin, M. Cormier, J. P. Adam, P. J. Metaxas, J. Ferré, *Europhys. Lett.* **2007**, *78*, 57007.
[129] T. Ha Pham, J. Vogel, J. Sampaio, M. Vaňatka, J.-C. Rojas-Sánchez, M. Bonfim, D. S. Chaves, F. Choueikani, P. Ohresser, E. Otero, A. Thiaville, S. Pizzini, *Europhys. Lett.* **2016**, *113*, 67001.
[130] E. Haltz, J. Sampaio, S. Krishnia, L. Berges, R. Weil, A. Mougin, *Sci. Rep.* **2020**, *10*, 16292.
[131] C. Kim, S. Lee, H. G. Kim, J. H. Park, K. W. Moon, J. Y. Park, J. M. Yuk, K. J. Lee, B. G. Park, S. K. Kim, K. J. Kim, C. Hwang, *Nat. Mater.* **2020**, *19*, 980.
[132] T. T. Liu, Y. Liu, Z. Jin, Z. P. Hou, D. Y. Chen, Z. Fan, M. Zeng, X. B. Lu, X. S. Gao, M. H. Qin, J.-M. Liu, *Phys. Rev. B* **2022**, *105*, 214432.
[133] S. Woo, K. M. Song, X. Zhang, Y. Zhou, M. Ezawa, X. Liu, S. Finizio, J. Raabe, N. J. Lee, S. I. Kim, S. Y. Park, Y. Kim, J. Y. Kim, D. Lee, O. Lee, J. W. Choi, B. C. Min, H. C. Koo, J. Chang, *Nat. Commun.* **2018**, *9*, 9.
[134] Y. Hirata, D. H. Kim, S. K. Kim, D. K. Lee, S. H. Oh, D. Y. Kim, T. Nishimura, T. Okuno, Y. Futakawa, H. Yoshikawa, A. Tsukamoto, Y. Tserkovnyak, Y. Shiota, T. Moriyama, S. B. Choe, K. J. Lee, T. Ono, *Nat. Nanotechnol.* **2019**, *14*, 232.
[135] T. Okuno, D.-H. Kim, S.-H. Oh, S. K. Kim, Y. Hirata, T. Nishimura, W. S. Ham, Y. Futakawa, H. Yoshikawa, A. Tsukamoto, Y. Tserkovnyak, Y. Shiota, T. Moriyama, K.-J. Kim, K.-J. Lee, T. Ono, *Nat. Electron.* **2019**, *2*, 389.
[136] D.-H. Kim, D.-H. Kim, K.-J. Kim, K.-W. Moon, S. Yang, K.-J. Lee, S. K. Kim, *J. Magn. Magn. Mater.* **2020**, *514*, 167237.
[137] W. H. Li, Z. Jin, D. L. Wen, X. M. Zhang, M. H. Qin, J.-M. Liu, *Phys. Rev. B* **2020**, *101*, 024414.
[138] B. Dieny, I. L. Prejbeanu, K. Garello, P. Gambardella, P. Freitas, R. Lehndorff, W. Raberg, U. Ebels, S. O. Demokritov, J. Akerman, A. Deac, P. Pirro, C. Adelmann, A. Anane, A. V. Chumak, A. Hirohata, S. Mangin, S. O. Valenzuela, M. C. Onbaşlı, M. D'Aquino, G. Prenat, G. Finocchio, L. Lopez-Diaz, R. Chantrell, O. Chubykalo-Fesenko, P. Bortolotti, *Nat. Electron.* **2020**, *3*, 446.
[139] L. Caretta, S.-H. Oh, T. Fakhrul, D.-K. Lee, B. H. Lee, S. K. Kim, C. A. Ross, K.-J. Lee, G. S. D. Beach, *Science* **2020**, *370*, 1438.
[140] T. H. Pham, S.-G. Je, P. Vallobra, T. Fache, D. Lacour, G. Malinowski, M. C. Cyrille, G. Gaudin, O. Boulle, M. Hehn, J.-C. Rojas-Sánchez, S. Mangin, *Phys. Rev. Appl.* **2018**, *9*, 064032.

[141] Z. Zheng, Z. Zhang, X. Feng, K. Zhang, Y. Zhang, Y. He, L. Chen, K. Lin, Y. Zhang, P. Khalili Amiri, W. Zhao, *ACS Nano* **2022**, *16*, 8264.
[142] J. Yu, D. Bang, R. Mishra, R. Ramaswamy, J. H. Oh, H.-J. Park, Y. Jeong, P. Van Thach, D.-K. Lee, G. Go, S.-W. Lee, Y. Wang, S. Shi, X. Qiu, H. Awano, K.-J. Lee, H. Yang, *Nat. Mater.* **2019**, *18*, 29.
[143] Y. Lim, B. Khodadadi, J.-F. Li, D. Viehland, A. Manchon, S. Emori, *Phys. Rev. B* **2021**, *103*, 024443.
[144] A. S. Núñez, R. A. Duine, P. Haney, A. H. MacDonald, *Phys. Rev. B* **2006**, *73*, 214426.
[145] T. Devolder, J. Hayakawa, K. Ito, H. Takahashi, S. Ikeda, P. Crozat, N. Zerounian, J.-V. Kim, C. Chappert, H. Ohno, *Phys. Rev. Lett.* **2008**, *100*, 057206.
[146] A. van den Brink, S. Cosemans, S. Cornelissen, M. Manfrini, A. Vaysset, W. Van Roy, T. Min, H. J. M. Swagten, B. Koopmans, *Appl. Phys. Lett.* **2014**, *104*, 012403.
[147] K.-J. J. K.-S. S. Lee, S.-W. W. Lee, B.-C. C. Min, K.-J. J. K.-S. S. Lee, *Appl. Phys. Lett.* **2013**, *102*, 112410.
[148] E. Martinez, L. Torres, N. Perez, M. A. Hernandez, V. Raposo, S. Moretti, *Sci. Rep.* **2015**, *5*, 10156.
[149] N. Mikuszeit, O. Boulle, I. M. Miron, K. Garello, P. Gambardella, G. Gaudin, L. D. Buda-Prejbeanu, *Phys. Rev. B* **2015**, *92*, 144424.
[150] C. Hahn, G. Wolf, B. Kardasz, S. Watts, M. Pinarbasi, A. D. Kent, *Phys. Rev. B* **2016**, *94*, 214432.
[151] J. Stöhr, H. C. Siegmann, *Magnetism*, Vol. *152*, Springer, Berlin **2006**.
[152] C. Bellouard, H. D. Rapp, B. George, S. Mangin, G. Marchal, J. C. Ousset, *Phys. Rev. B* **1996**, *53*, 5082.
[153] W. Zhou, T. Seki, T. Kubota, G. E. Bauer, K. Takanashi, *Phys. Rev. Mater.* **2018**, *2*, 094404.
[154] M. Beens, M. L. M. Lalieu, R. A. Duine, B. Koopmans, *AIP Adv.* **2019**, *9*, 125133.
[155] I. Radu, K. Vahaplar, C. Stamm, T. Kachel, N. Pontius, H. A. Dürr, T. A. Ostler, J. Barker, R. F. L. Evans, R. W. Chantrell, A. Tsukamoto, A. Itoh, A. Kirilyuk, T. Rasing, A. V. Kimel, *Nature* **2011**, *472*, 205.
[156] T. A. Ostler, J. Barker, R. F. Evans, R. W. Chantrell, U. Atxitia, O. Chubykalo-Fesenko, S. El Moussaoui, L. Le Guyader, E. Mengotti, L. J. Heyderman, F. Nolting, A. Tsukamoto, A. Itoh, D. Afanasiev, B. A. Ivanov, A. M. Kalashnikova, K. Vahaplar, J. Mentink, A. Kirilyuk, T. Rasing, A. V. Kimel, *Nat. Commun.* **2012**, *3*, 666.
[157] A. Kirilyuk, A. V. Kimel, T. Rasing, *Rep. Prog. Phys.* **2013**, *76*, 026501.
[158] R. Asomoza, I. A. Campbell, H. Jouve, R. Meyer, *J. Appl. Phys.* **1977**, *48*, 3829.
[159] R. Malmhäll, *J. Appl. Phys.* **1983**, *54*, 5128.
[160] X. Jiang, L. Gao, J. Z. Sun, S. S. P. Parkin, *Phys. Rev. Lett.* **2006**, *97*, 217202.
[161] K. Ueda, C.-f. Pai, A. J. Tan, M. Mann, G. S. D. Beach, *Appl. Phys. Lett.* **2016**, *108*, 232405.
[162] N. Reynolds, P. Jadaun, J. T. Heron, C. L. Jermain, J. Gibbons, R. Collette, R. A. Buhrman, D. G. Schlom, D. C. Ralph, *Phys. Rev. B* **2017**, *95*, 064412.
[163] Q. Wong, C. Murapaka, W. Law, W. Gan, G. Lim, W. Lew, *Phys. Rev. Appl.* **2019**, *11*, 024057.
[164] M. Martini, C. O. Avci, S. Tacchi, C.-h. Lambert, P. Gambardella, *Phys. Rev. Appl.* **2022**, *17*, 044056.
[165] A. Yagmur, S. Sumi, H. Awano, K. Tanabe, *Phys. Rev. B* **2021**, *103*, 214408.
[166] R. Q. Zhang, L. Y. Liao, X. Z. Chen, T. Xu, L. Cai, M. H. Guo, H. Bai, L. Sun, F. H. Xue, J. Su, X. Wang, C. H. Wan, H. Bai, Y. X. Song, R. Y. Chen, N. Chen, W. J. Jiang, X. F. Kou, J. W. Cai, H. Q. Wu, F. Pan, C. Song, *Phys. Rev. B* **2020**, *101*, 214418.
[167] J. W. Lee, J. Y. Park, J. M. Yuk, B.-G. Park, *Phys. Rev. Appl.* **2020**, *13*, 044030.
[168] D. Céspedes-Berrocal, H. Damas, S. Petit-Watelot, D. Maccariello, P. Tang, A. Arriola-Córdova, P. Vallobra, Y. Xu, J. Bello, E. Martin, S. Migot, J. Ghanbaja, S. Zhang, M. Hehn, S. Mangin, C. Panagopoulos, V. Cros, A. Fert, J. Rojas-Sánchez, *Adv. Mater.* **2021**, *33*, 2007047.
[169] C. Kaiser, A. F. Panchula, S. S. P. Parkin, *Phys. Rev. Lett.* **2005**, *95*, 047202.
[170] J. Y. Chen, L. He, J. P. Wang, M. Li, *Phys. Rev. Appl.* **2017**, *7*, 2.
[171] L. Avilés-Félix, L. Álvaro-Gómez, G. Li, C. S. Davies, A. Olivier, M. Rubio-Roy, S. Auffret, A. Kirilyuk, A. V. Kimel, T. Rasing, L. D. Buda-Prejbeanu, R. C. Sousa, B. Dieny, I. L. Prejbeanu, *AIP Adv.* **2019**, *9*, 125328.
[172] C. Banerjee, N. Teichert, K. E. Siewierska, Z. Gercsi, G. Y. P. Atcheson, P. Stamenov, K. Rode, J. M. D. Coey, J. Besbas, *Nat. Commun.* **2020**, *11*, 4444.
[173] J. Jeong, Y. Ferrante, S. V. Faleev, M. G. Samant, C. Felser, S. S. P. Parkin, *Nat. Commun.* **2016**, *7*, 10276.
[174] C. O. Avci, A. Quindeau, C.-F. Pai, M. Mann, L. Caretta, A. S. Tang, M. C. Onbasli, C. A. Ross, G. S. D. Beach, *Nat. Mater.* **2017**, *16*, 309.
[175] C. O. Avci, E. Rosenberg, L. Caretta, F. Büttner, M. Mann, C. Marcus, D. Bono, C. A. Ross, G. S. D. Beach, *Nat. Nanotechnol.* **2019**, *14*, 561.
[176] S. Vélez, J. Schaab, M. S. Wörnle, M. Müller, E. Gradauskaite, P. Welter, C. Gutgsell, C. Nistor, C. L. Degen, M. Trassin, M. Fiebig, P. Gambardella, *Nat. Commun.* **2019**, *10*, 4750.
[177] S. Ghosh, T. Komori, A. Hallal, J. Peña Garcia, T. Gushi, T. Hirose, H. Mitarai, H. Okuno, J. Vogel, M. Chshiev, J.-P. Attané, L. Vila, T. Suemasu, S. Pizzini, *Nano Lett.* **2021**, *21*, 2580.

Giacomo Sala is a Ph.D. candidate in the Magnetism and Interface Physics group of the Department of Materials at ETH Zurich. He graduated in Engineering Physics at Politecnico di Milano, Italy, and joined soon after Prof. Gambardella's group. His experimental activity focuses on the GHz magnetization dynamics induced by spin-orbit torques in ferro- and ferrimagnets, harmonic measurements of spin-orbit torques and magnetoresistance effects, and the current-induced orbital Hall effect.

Pietro Gambardella is Professor and Chair of Magnetism and Interface Physics at the Department of Materials, ETH Zurich. He graduated in Physics from the University of Genova, Italy, and received his Ph.D. from the Ecole Polytechnique Fédérale de Lausanne, Switzerland. Prof. Gambardella's research interests include investigating the magnetic and electronic properties of thin film heterostructures, spintronic devices, single atom and molecule magnets, and the development of techniques to perform time- and frequency-resolved magnetization measurements.